CHAPTER 2

From upscaling techniques to hybrid models

I. Battiato & D.M. Tartakovsky

2.1 INTRODUCTION

Any mathematical model is an idealization of a real system at a specified scale. Assumptions and/or simplifications upon which such models are based enable their formulation, analytical and/or numerical treatment and, consequently, their use as predictive tools. The acceptance of a model derives from an optimal balance between simplicity and accuracy in capturing a system's behavior on the one hand and computational costs on the other. Different models might offer optimal performances, both in terms of fidelity and computation, in various regimes. A further complication in model selection arises when a scale at which predictions are sought is much larger than a scale at which governing equations and first principles are well defined. This situation is particularly common in analysis of flow and transport in porous media: typical scales of interest for predictions are often many orders of magnitude larger than a scale at which most biochemical processes take place. Such complex systems are of particular interest because of their ubiquitous nature: they characterize a variety of environments ranging from geologic formations to biological cells, and from oil reservoirs to nanotechnology products.

Flow and transport in porous media can be modeled at the pore- (microscopic) or Darcy- (macroscopic) scales. Equations that have a solid physical foundation and are based on the first principles (e.g., Stokes' equations for fluid flow and Fick's law of diffusion for solute transport) require the knowledge of pore geometry that is seldom available in real applications. While rapid advancements in computational power and imagine techniques bode well for the widespread use of pore-scale models at increasingly larger scales, computational domains that can be modeled with modern-day pore-scale simulations are still too small to be of any use for predictions at the field scale: the heterogeneity of most natural porous media (e.g., oil reservoirs and aquifers) and technology products (carbon nanotubes assemblies) and prohibitive computational costs render lattice-Boltzmann modeling (Leemput et al. 2007), smoothed particle hydrodynamics (Tartakovsky et al. 2007), molecular dynamics (Walther et al. 2004) and other pore-scale simulations impractical as a predictive tool at scales that are many orders of magnitude larger than the pore scale.

Macroscopic models (e.g., Darcy's law for fluid flow and an advection-dispersion equation for transport), which treat a porous medium as an "averaged" continuum, overcome these limitations by relying on phenomenological descriptions and a number of simplifications (e.g., spatial smoothness of pore-scale quantities, spatial periodicity of pore structures, and low degree of physical and chemical heterogeneity).

The ubiquitous presence of heterogeneities in natural systems might lead to a localized breakdown of such continuum models. Whenever a *localized* breakdown of continuum-scale models occurs, hybrid models must be used to attain an increased rigor and accuracy in predictions, while keeping computational costs in check. Hybrid simulations (Leemput et al. 2007, Tartakovsky et al. 2007) resolve a small reactive region with a pore-scale model that is coupled to its continuum counterpart in the rest of a computational domain.

In Section 2.2 we present a classification of the most common upscaling methods (Section 2.2.1), which allow one to derive macroscopic equations from their pore-scale counterparts. Sections 2.2.2 and 2.2.3 contain classical results of homogenization theory and their

implications for applicability of macroscopic models. In Section 2.3 we identify the applicability range of macroscopic models for diffusive systems with nonlinear homogeneous reaction (Section 2.3.1) and advective-diffusive systems with nonlinear heterogeneous reactions (Section 2.3.4). In Section 2.4 we use volume averaging to construct the formalism of two types of hybrid algorithms, intrusive (Section 2.4.1) and non-intrusive (Section 2.4.5). Our major conclusions are presented in Section 2.5.

2.2 FROM FIRST PRINCIPLES TO EFFECTIVE EQUATIONS

2.2.1 *Classification of upscaling methods*

We consider a porous medium $\Omega = \Omega_s \cup \Omega_l$ consisting of a solid matrix Ω_s and a fluid-filled pore space Ω_l. A major goal of upscaling is to establish connections between pore- and continuum-scale descriptions of transport processes in Ω. Mathematical approaches to upscaling include the method of volume averaging (Whitaker 1999) and its modifications (Kechagia et al. 2002), generalizations of the method of moments (Shapiro & Brenner 1986, 1988, Shapiro et al. 1996), homogenization via multiple-scale expansions (Adler 1992), pore-network models (Acharya et al. 2005), and thermodynamically constrained averaging (Gray & Miller 2005).

Let u be a real-valued function on a pore-scale domain Ω_l that exhibits rapid spatial oscillations. It describes a certain physical quantity and satisfies a partial differential equation:

$$\mathscr{L}[u] = f \tag{2.1}$$

One can define the local average of u as:

$$\langle u \rangle(\mathbf{x}) = \frac{1}{|\mathscr{V}|} \int_{\mathscr{V}(\mathbf{x})} u(\mathbf{y})\, \mathrm{d}\mathbf{y} \tag{2.2}$$

In the method of volume averaging, the support volume $\mathscr{V}$ "is a small, but not too small, neighborhood of point $\mathbf{x}$ of the size of a representative elementary volume, REV (several hundred or thousand of pores)" (Hornung 1997, p. 1). The ambiguity in defining the size of an REV is typical. For example, in (de Marsily 1986, p. 15) "the size of the REV is defined by saying that it is

- sufficiently large to contain a great number of pores so as to allow us to define a mean global property, while ensuring that the effects of the fluctuations from one pore to another are negligible. One may take, for example, 1 cm^3 or 1 dm^3;
- sufficiently small so that the parameter variations from one domain to the next may be approximated by continuous functions, in order that we may use infinitesimal calculus."

A continuum-scale equation:

$$\overline{\mathscr{L}}[\langle c \rangle] = g, \tag{2.3}$$

is constructed by volumetric averaging of the original pore-scale equation (Eq. 2.1). The procedure is facilitated by the spatial averaging theorem, which enables one to exchange spatial integration and differentiation (Whitaker 1999):

$$\langle \nabla u \rangle = \nabla \langle u \rangle + \frac{1}{|\mathscr{V}|} \int_{A_{ls}} u\mathbf{n}\, \mathrm{d}A, \tag{2.4}$$

where A_{ls} is the liquid-solid interface contained in $\mathscr{V}$ and $\mathbf{n}$ is the outward normal unit vector of A_{ls}.

Similar concepts are used in thermodynamically constrained averaging theory (Gray & Miller 2005), wherein thermodynamics is introduced into a constrained entropy inequality to guide the formation of closed macroscale models that retain consistency with microscale physics and thermodynamics.

In the homogenization theory by multiple-scale expansions (Hornung 1997), the volume $\mathscr{V}$ is the unit cell of a periodic porous medium Ω with period ϵ. A homogenized equation is obtained by determining the following limit:

$$\langle u \rangle = \langle \lim_{\epsilon \to 0} u_\epsilon \rangle, \tag{2.5}$$

where u_ϵ is the sequence (indexed by ϵ) of solutions of Eq. (2.1) with periodically oscillating coefficients. The limit is determined by utilizing a two-scale asymptotic expansion that "is an ansatz of the form:

$$u_\epsilon(\mathbf{x}) = u_0(\mathbf{x}, \mathbf{x}/\epsilon) + \epsilon u_1(\mathbf{x}, \mathbf{x}/\epsilon) + \epsilon^2 u_2(\mathbf{x}, \mathbf{x}/\epsilon) + \cdots \tag{2.6}$$

where each function $u_i(\mathbf{x}, \mathbf{y})$ in this series depends on two variables, $\mathbf{x}$ the macroscopic (or slow) variable and $\mathbf{y}$ the microscopic (or fast) variable, and is $\mathscr{V}$-periodic in $\mathbf{y}$ ($\mathscr{V}$ is the unit period). Inserting Eq. (2.6) into Eq. (2.1) satisfied by u_ϵ and identifying powers of ϵ leads to a cascade of equations for each term $u_i(\mathbf{x}, \mathbf{y})$. In general averaging with respect to $\mathbf{y}$ yields the homogenized equation for u_0. Another step is required to rigorously justify the homogenization result obtained heuristically with this two-scale asymptotic expansion" (Hornung 1997, p. 238).

Similar to the homogenization theory definition of average is that of the methods of moments, wherein the global ($\mathbf{x}$) and local ($\mathbf{y}$) variables "characterize the instantaneous position (configuration) of the Brownian particle in its phase space. Together the vectors $(\mathbf{x}, \mathbf{y})$ define a multidimensional phase space $\mathbf{x} \oplus \mathbf{y}$ within which convective and diffusive solute-particle transport processes occur. The domain of permissible values of $\mathbf{x}$ will always be unbounded; in contrast, the domain of permissible or accessible values of $\mathbf{y}$ will generally be bounded" (Brenner 1987, pp. 66–67), i.e., $\mathbf{y} \in \mathscr{V}$. In this case, a macroscopic transport equation is obtained for the probability density function of a Brownian particle (Brenner 1987, Equations 3.3–3.5):

$$\overline{P}(\mathbf{x}, t|\mathbf{y}') \stackrel{def}{=} \int_{\mathscr{V}} P(\mathbf{x}, \mathbf{y}, t|\mathbf{y}')\, \mathrm{d}\mathbf{y} \tag{2.7}$$

where $P(\mathbf{x}, \mathbf{y}, t|\mathbf{y}') \equiv P(\mathbf{x} - \mathbf{x}', \mathbf{y}, t - t'|\mathbf{y}')$ with $\mathbf{x}' = \mathbf{0}$ and $t' = 0$ denotes the "conditional probability density that the Brownian particle is situated at position $(\mathbf{x}, \mathbf{y})$ at time t, given that it was initially introduced into the system at the position $(\mathbf{x}', \mathbf{y}')$ at some earlier time t' $(t > t')$" (Brenner 1987, p. 68). "For sufficiently long times (i.e. 'long' relative to the time scale of evolution of the microscale transport process, but 'short' relative to the time scale of the macrotransport process) we expect that the particle(s) will loose memory of the initial position(s) $\mathbf{y}'$". Consequently, $\overline{P}(\mathbf{x}, t|\mathbf{y}') \approx \overline{P}(\mathbf{x}, t)$ and a fully macrotransport equation can be determined.

A number of other approaches to upscaling are reviewed by Brenner (1987). Even if based on different definitions of the averaging volume and on distinct mathematical tools, all upscaling methods require closure assumptions to decouple the average system behavior from the pore-scale information: the latter is exclusively incorporated into the upscaled equation through effective parameters that can be determined by laboratory experiments or numerical solution of a closure problem at the unit cell level.

2.2.2 *Flow: From Stokes to Darcy/Brinkman equations*

Single-phase flow of an incompressible Newtonian fluid in porous media in the pore-space Ω_l is described by the Stokes and continuity equations subject to the no-slip boundary condition on A_{ls}:

$$\mu \nabla^2 \mathbf{v} - \nabla p = 0, \quad \nabla \cdot \mathbf{v} = 0, \quad \mathbf{x} \in \Omega_l, \qquad \mathbf{v} = \mathbf{0}, \quad \mathbf{x} \in A_{ls}, \tag{2.8}$$

where $\mathbf{v}(\mathbf{x})$ is the fluid velocity, p denotes the fluid dynamic pressure, and μ is the dynamic viscosity.

Upscaling of the Stokes equations (Eq. 2.8) at the pore-scale to the continuum scale has been the subject of numerous investigations, including those relying on multiple-scale expansions (Sanchez-Palencia & Zaoui 1989, Hornung 1997, Auriault & Adler 1995, Mikelić et al. 2006, Peter 2007, Marušić-Paloka & Piatnitski 2005, and references therein), volume averaging (Neuman 1977, and references therein), the method of moments, etc. These studies have demonstrated that Darcy's law, which was empirically established by Darcy (1856), and the continuity equation for $\langle \mathbf{v} \rangle$:

$$\langle \mathbf{v} \rangle = -\frac{\mathbf{K}}{\mu} \cdot \nabla \langle p \rangle, \qquad \nabla \cdot \langle \mathbf{v} \rangle = 0, \qquad \mathbf{x} \in \Omega, \tag{2.9}$$

provide an effective representation of the pore-scale Stokes flow (Hornung 1997, Eq. 4.7). Such upscaling procedures also enable one to formally define the permeability tensor $\mathbf{K}$ in Eq. (2.9) as the average of a "closure variable" $\mathbf{k}(\mathbf{y})$, i.e., $\mathbf{K} = \langle \mathbf{k}(\mathbf{y}) \rangle$. The latter is the unique solution of a local problem (e.g., Hornung 1997, pp. 46–47, Theorem 1.1 and Auriault & Adler 1995, Eq. 22) defined on a representative (unit) cell of the porous medium. "It is well admitted that the existence of continuum behaviors that are macroscopically equivalent to finely heterogeneous media needs a good separation of scales. If l and L are the characteristic lengths at the local and the macroscopic scale, respectively, their ratio should obey" (Auriault et al. 2005):

$$\epsilon = \frac{l}{L} \ll 1, \tag{2.10}$$

To describe flow through "hyperporous" media, Brinkman (1949) introduced a modification of Darcy's law:

$$\nabla \langle p \rangle = -\frac{\mu}{\mathbf{K}} \langle \mathbf{v} \rangle + \mu_e \nabla^2 \langle \mathbf{v} \rangle, \tag{2.11}$$

where μ_e is an effective viscosity "which may differ from μ" (Brinkman 1949). The *raison d'etre* for such a modification was the necessity of obtaining an equation that was valid in the high permeability limit ($|\mathbf{K}| \to \infty$) and that allowed for a direct coupling with the Stokes equations at interfaces separating Stokes flow (infinite permeability regions) and filtration flow (low permeability regions). In Brinkman's words, "this equation has the advantage of approximating Eq. (2.9) for low values of $\mathbf{K}$ and Eq. (2.8) for high values of $\mathbf{K}$".

After its introduction and its widespread use, an increasing research effort was devoted to the identification of domains of validity of both Darcy's & Brinkman's law (Lévy 1983, Auriault 2009, Durlofsky & Brady 2009, and references therein). Brinkman's intuition was mathematically proven later by Goyeau et al. (1997) and Auriault et al. (2005), who used respectively the method of volume averaging and multiple-scale expansions to demonstrate that Brinkman's equation represents a higher-order approximation of Darcy's law when the separation of scales is poor.

2.2.3 *Transport: From advection-diffusion to advection-dispersion equation*

Consider a fluid that contains a dissolved species $\mathcal{M}$, whose dimensional concentration $c(\mathbf{x}, t)$ $[molL^{-3}]$ at point $\mathbf{x} \in \Omega_l$ and time $t > 0$ changes due to advection, molecular diffusion, homogeneous reaction in the liquid phase and heterogeneous reaction at the solid-liquid interface A_{ls}. The first three phenomena are described by an advection-diffusion-reaction equation:

$$\frac{\partial c}{\partial t} + \mathbf{v} \cdot \nabla c = \nabla \cdot (\mathbf{D} \nabla c) + R(c), \qquad \mathbf{x} \in \Omega_l, \quad t > 0, \tag{2.12}$$

where the molecular diffusion coefficient $\mathbf{D}$ is, in general, a positive-definite second-rank tensor. If diffusion is isotropic, $\mathbf{D} = \mathscr{D}\mathbf{I}$ where $\mathscr{D}$ $[L^2T^{-1}]$ is the diffusion coefficient and $\mathbf{I}$ is the identity matrix. The source term $R(c)$ represents a generic homogeneous reaction. At the solid-liquid interface A_{ls} impermeable to flow, mass conservation requires that mass flux of the species $\mathcal{M}$ be balanced by net mass flux due to heterogeneous reaction, $Q(c)$:

$$-\mathbf{n} \cdot \mathbf{D} \nabla c = Q(c), \qquad \mathbf{x} \in A_{ls}, \tag{2.13}$$

In addition to Eq. (2.13), the flow and transport equations, Eq. (2.8) and Eq. (2.12), are supplemented with boundary conditions on the external boundary of the flow domain Ω. The upscaling of Eq. (2.12) and Eq. (2.13) leads to effective equations for the average concentration $\langle c \rangle$, generally written in the following form:

$$\frac{\partial \langle c \rangle}{\partial t} + \langle \mathbf{v} \rangle \cdot \nabla \langle c \rangle = \nabla \cdot (\mathbf{D}^* \nabla \langle c \rangle) + \overline{R}(\langle c \rangle) + \overline{Q}(\langle c \rangle), \qquad \mathbf{x} \in \Omega, \quad t > 0, \tag{2.14}$$

where $\mathbf{D}^*$ is a dispersion tensor and $\overline{R}(\langle c \rangle)$ and $\overline{Q}(\langle c \rangle)$ are effective reactive sources.

A significant research effort and ingenuity has been devoted to the upscaling of various functional forms of $R(c)$ and $Q(c)$ relevant to engineering, chemical, biochemical, hydrological, and other applications (Shapiro & Brenner 1986, 1988, Ochoa-Tapia et al. 1991, Shapiro et al. 1996, Wood & Ford 2007, Wood et al. 2007, van Noorden & Pop 2008, Hesse et al. 2009). Yet, very little, and only recent, attention has been paid to the identification of the applicability conditions of the upscaled models proposed by such a prolific research path.

While useful in a variety of applications, continuum models fail to capture experimentally observed transport features, including a difference between fractal dimensions of the diffusion and dispersion fronts (isoconcentration contours) (Maloy et al. 1998), long tails in breakthrough curves (Neuman & Tartakovsky 2009), and the onset of instability in variable density flows (Tartakovsky et al. 2008b). ADE-based models of transport of (bio-)chemically reactive solutes, which are the focus of our analysis, can significantly over-predict the extent of reactions in mixing-induced chemical transformations (Knutson et al. 2007, Wood et al. 2007, Tartakovsky et al. 2007, Li et al. 2006, Tartakovsky et al. 2008a, and references therein). These and other shortcomings stem from the inadequacy of either standard macroscopic models or their parametrizations or both. Upscaling from the pore-scale, on which governing equations are physically based and well defined, to the continuum scale, on which they are used for qualitative predictions, often enables one to establish the connection between the two modeling scales.

Upscaling approaches that rely on characteristic dimensionless numbers (e.g., the Damköhler and Péclet numbers) can provide quantitative measures for the validity of various upscaling approximations. Auriault and Adler (1995) used multiple scale expansions to establish the applicability range of advection-dispersion equation for a non-reactive solute in terms of Péclet number. Mikelić et al. (2006) provided a rigorous upscaled version of the Taylor dispersion problem with linear heterogeneous reaction. For flow between two parallel reacting plates they established the applicability range of the upscaled equation in terms of the Damköhler and Péclet numbers.

Nonlinearity of governing equations complicates the upscaling of most reactive transport phenomena. It requires a linearization and/or other approximations, whose accuracy and validity cannot be ascertained a priori. This is especially so for a large class of transport processes, such as mixing-induced precipitation, which exhibit highly localized reacting fronts and consequently defy macroscopic descriptions that are completely decoupled from their microscopic counterparts (Ochoa-Tapia et al. 1991, Auriault & Adler 1995, Kechagia et al. 2002).

In the following section, we present results from Battiato et al. (2009) and Battiato and Tartakovsky (2010) that generalize the analyses of Auriault and Adler (1995) and Mikelić et al. (2006) to nonlinear reactive processes. In Section 2.3.1 we consider a multicomponent system undergoing nonlinear homogeneous and linear heterogeneous reaction described by a system of coupled reaction-diffusion equations (RDEs); we specify key physical and (bio-)chemical assumptions that underpin this model and identify the Damköhler numbers for homogeneous and heterogeneous reactions as dimensionless parameters that control the phenomenon. We present the major results of volume averaging (Whitaker 1999) pore-scale equations to derive a system of upscaled RDEs that are commonly used to model mixing-induced precipitation on the continuum scale (e.g., Steefel et al. 2005, and the references therein). The goal here is to identify sufficient conditions for the macroscopic RDEs to be a valid descriptor of mixing-induced precipitation. To focus on the relative effects of nonlinear geochemical reactions and diffusion, we neglect advection.

In Section 2.3.4 we consider the advective-diffusive transport of a solute that undergoes a nonlinear heterogeneous reaction: after reaching a threshold concentration value, it precipitates

on the solid matrix to form a crystalline solid. The relative importance of three key pore-scale transport mechanisms (advection, molecular diffusion, and reactions) is quantified by the Péclet (*Pe*) and Damköhler (*Da*) numbers. We use multiple-scale expansions to upscale a pore-scale advection-diffusion equation with reactions entering through a boundary condition on the fluid-solid interface, and to establish sufficient conditions under which macroscopic advection-dispersion-reaction equations (ADREs) provide an accurate description of the pore-scale processes. These conditions are summarized by a phase diagram in the (*Pe*, *Da*) space, parameterized with a scale-separation parameter that is defined as the ratio of characteristic lengths associated with the pore- and macro-scales.

2.3 APPLICABILITY RANGE OF MACROSCOPIC MODELS FOR REACTIVE SYSTEMS

2.3.1 *Diffusion-reaction equations: mixing-induced precipitation processes*

Consider a porous medium Ω that is fully saturated with an incompressible liquid at rest. The liquid, occupying the pore-space Ω_l, is a solution of two chemical (or biological) species M_1 and M_2 (with respective concentrations c_1 and c_2) that react to form an aqueous reaction product M_3. Whenever c_3, the concentration of M_3, exceeds a threshold value, M_3 undergoes a heterogeneous reaction and precipitates on the solid matrix, forming a precipitate $M_{4(s)}$. In general, this process of mixing-induced precipitation is fully reversible, $M_1 + M_2 \rightleftarrows M_3 \rightleftarrows M_{4(s)}$, and its speed is controlled by the reaction rates k_{12} $[L^3 mol^{-1} T^{-1}]$, k_p $[LT^{-1}]$, k_3 $[T^{-1}]$ and k_d $[molT^{-1}L^{-2}]$ corresponding to the following reactions:

$$M_1 + M_2 \xrightarrow{k_{12}} M_3 \xrightarrow{k_p} M_{4(s)} \quad \text{and} \quad M_1 + M_2 \xleftarrow{k_3} M_3 \xleftarrow{k_d} M_{4(s)} \tag{2.15}$$

For bimolecular and unimolecular elementary reactions at constant temperature, the change in concentration is proportional to the product of the concentration of the reactants. Hence, the consumption and production rates, R_i^c with $i \in \{1, 2\}$ and R_3^p, of species M_i, $i \in \{1, 2\}$, and M_3, respectively, associated with the homogeneous reaction in Eq. (2.15) are typically concentration-driven and of the form $R_i^c = -R_3^p = -k_{12}\hat{c}_1\hat{c}_2 + k_3\hat{c}_3$. For the heterogeneous reaction, it is common to assume (Knabner et al. 1995, Duijn & Pop 2004, and references therein) that i) precipitation rate r_p is proportional to concentration $\hat{c}_3$, i.e., $r_p = k_p\hat{c}_3$; ii) dissolution rate r_d is constant, $r_d = k_d$; and iii) super-saturation index does not become large enough to support precipitation in the liquid phase, i.e., precipitation of M_3 occurs solely as an overgrowth on solid grains.

With these assumptions, the aqueous concentrations $\hat{c}_i(\hat{\mathbf{r}}, \hat{t})$ $\left[molL^{-3}\right]$ at point $\hat{\mathbf{r}}$ and time $\hat{t}$ satisfy a system of reaction-diffusion equations (RDEs):

$$\frac{\partial \hat{c}_i}{\partial \hat{t}} = \mathscr{D}_i \hat{\nabla}^2 \hat{c}_i - k_{12}\hat{c}_1\hat{c}_2 + k_3\hat{c}_3 \quad \text{for } \hat{\mathbf{r}} \in \Omega_l, \hat{t} > 0 \quad i = 1, 2 \tag{2.16a}$$

$$\frac{\partial \hat{c}_3}{\partial \hat{t}} = \mathscr{D}_3 \hat{\nabla}^2 \hat{c}_3 + k_{12}\hat{c}_1\hat{c}_2 - k_3\hat{c}_3 \quad \text{for } \hat{\mathbf{r}} \in \Omega_l, \hat{t} > 0, \tag{2.16b}$$

subject to the boundary conditions on the (multi-connected) liquid-solid interface $\mathscr{A}_{ls}$:

$$\mathbf{n} \cdot \hat{\nabla}\hat{c}_i = 0, \quad i = 1, 2; \qquad -\mathscr{D}_3 \mathbf{n} \cdot \hat{\nabla}\hat{c}_3 = k_p(\hat{c}_3 - c_{\text{eq}}) \tag{2.17}$$

and the initial conditions:

$$\hat{c}_i(\mathbf{x}, 0) = c_{i0}(\mathbf{x}), \quad i = 1, 2, 3, \qquad \Omega_l(0) = \Omega_{l0}, \tag{2.18}$$

when concentration of $M_{4(s)}$ is strictly positive. Here the hatted quantities have appropriate units (physical dimensions), $c_{\text{eq}} = k_d/k_p$ is the equilibrium concentration, $\mathscr{D}_i$ $[L^2T^{-1}]$ $(i = 1, 2, 3)$ are the diffusion coefficients of the aqueous species M_1, M_2, and M_3, respectively. Due to

precipitation and dissolution, the liquid-solid interface $\mathscr{A}_{ls}(\hat{t})$, with the outward normal unit vector $\mathbf{n}(\hat{t})$, evolves in time $\hat{t}$ with velocity $\mathbf{v}$ $[LT^{-1}]$, according to $\rho_c \mathbf{v} \cdot \mathbf{n} = k_p(\hat{c}_3 - c_{\text{eq}})$, where ρ_c $[mol_s L^{-3}]$ is the molar density of the precipitate. The dynamics of the interface $\mathscr{A}_{ls}(\hat{t})$, result from a modeling assumption about the dependence of $\mathbf{v}$ on precipitation/dissolution rates and mass conservation (van Noorden & Pop 2008).

To be specific, we consider a scenario in which two identical solvents (e.g., water), one containing M_1 with concentration $\hat{c}_{10}$ and the other containing M_2 with concentration $\hat{c}_{20}$, are brought in contact with each other at time $\hat{t} = 0$. Since reactants M_1 and M_2 are initially separated, no reactions took place and the initial concentration of reaction product M_3 is $\hat{c}_{30} = 0$. This is a typical situation, corresponding, for example, to injection of a solution of M_1 into a porous medium occupied by a solution of M_2 (Tartakovsky et al. 2008a).

The characteristic time scales associated with the chemical reactions Eq. (2.15) are $\tau_1 = \tau_2 = 1/k_{12}c_{10}$ for concentrations $\hat{c}_1$ and $\hat{c}_2$, and $\tau_3 = c_{\text{eq}}/k_{12}c_{10}^2$ for concentration $\hat{c}_3$. To simplify the presentation, we assume that the diffusion coefficients for reactants M_1 and M_2 and product $M_{3(l)}$ are the same, $\mathscr{D}_1 = \mathscr{D}_2 = \mathscr{D}_3 = \mathscr{D}$. Let us introduce dimensionless quantities:

$$t = \frac{\hat{t}}{\tau}, \quad q = \frac{c_{\text{eq}}}{c_{10}}, \quad c_i = \frac{\hat{c}_i}{c_{10}}, \quad c_3 = \frac{\hat{c}_3}{c_{\text{eq}}}, \quad K = \frac{k_3 c_{eq}}{k_{12}c_{10}^2}, \quad Da = \frac{l^2 k_{12} c_{10}}{\mathscr{D}}, \tag{2.19}$$

where $i = 1, 2$; l denotes a characteristic length scale associated with pore structure; and the Damköhler number Da is the ratio of diffusion and reaction time scales for species M_i $(i = 1, 2, 3)$. RDEs Eq. (2.16) can now be written in a dimensionless form as:

$$\frac{\partial c_i}{\partial t} = \frac{l^2}{Da}\hat{\nabla}^2 c_i - c_1 c_2 + K c_3 \ (i = 1, 2), \qquad q\frac{\partial c_3}{\partial t} = \frac{q l^2}{Da}\hat{\nabla}^2 c_3 + c_1 c_2 - K c_3, \tag{2.20}$$

Following Tartakovsky et al. (2007), we define the Damköhler number for the precipitation/dissolution process as:

$$Da_{ls} = \frac{k_p l}{\mathscr{D}}, \tag{2.21}$$

This yields a dimensionless form of the boundary conditions on the liquid-solid interface $\mathscr{A}_{ls}$:

$$\mathbf{n} \cdot \hat{\nabla} c_i = 0 \ (i = 1, 2), \quad \mathbf{n} \cdot l\hat{\nabla} c_3 = Da_{ls}(1 - c_3). \tag{2.22}$$

We proceed by employing the local volume averaging (Whitaker 1999) to upscale the pore-scale equations, Eq. (2.20) and Eq. (2.22) to the macroscopic scale. Section 2.3.2 contains definitions of the averaging procedure. The results of the upscaling procedure are presented in form of Propositions in Section 2.3.3 (Battiato et al. 2009). The results are summarized in a phase diagram identifying sufficient conditions under which the upscaled (macroscopic) description is valid.

2.3.2 *Preliminaries*

Consider a portion of the porous medium $\mathscr{V} \in \Omega$ whose volume is $|\mathscr{V}|$ and characteristic radius $r_0 \gg l$, where l is the pore-geometry length scale. Let $B(\hat{\mathbf{x}}) \in \mathscr{V}$ denote the volume of the liquid phase contained in $\mathscr{V}$, which is centered at $\hat{\mathbf{x}} \in \Omega$. If a characteristic length-scale of the macroscopic domain Ω is L, then the size of the averaging volume $\mathscr{V}$ is selected to satisfy $l \ll r_0 \ll L$.

Following Whitaker (1999), we define superficial and intrinsic averages of a quantity $c(\hat{\mathbf{r}})$ with $\hat{\mathbf{r}} \in \Omega_l$ as:

$$\langle c \rangle(\hat{\mathbf{x}}) = \frac{1}{|\mathscr{V}|}\int_{B(\hat{\mathbf{x}})} c(\hat{\mathbf{r}})\,\mathrm{d}^3 r \quad \text{and} \quad \langle c \rangle_B(\hat{\mathbf{x}}) = \frac{1}{|B(\hat{\mathbf{x}})|}\int_{B(\hat{\mathbf{x}})} c(\hat{\mathbf{r}})\,\mathrm{d}^3 r, \tag{2.23}$$

respectively. The two averages are related through porosity $\phi \equiv |B|/|\mathscr{V}|$ by $\langle c \rangle = \phi \langle c \rangle_B$. The application of spatial averaging is facilitated by the spatial averaging theorem Eq. (2.4).

Let L_c, L_{c1} and L_ϕ denote characteristic length-scales associated with the macroscopic quantities $\langle c\rangle_B$, $\hat{\nabla}\langle c\rangle_B$ and ϕ, respectively. These scales are defined by (Whitaker 1999, p. 19):

$$\hat{\nabla} f_i(x) = \mathcal{O}\left(\frac{\Delta f_i}{L_i}\right), \qquad \Delta f_i(x) \equiv f_i\left(x + \frac{L_i}{2}\right) - f_i\left(x - \frac{L_i}{2}\right) \tag{2.24}$$

for $f_i = \{\langle c\rangle_B, \hat{\nabla}\langle c\rangle_B, \phi\}$ and $L_i = \{L_c, L_{c1}, L_\phi\}$, respectively. The notation $f = \mathcal{O}(g)$ denotes an order of magnitude estimate in the following sense (Kundu & Cohen 2008, p. 391):

$$\frac{|g|}{\sqrt{10}} \leq |f| \leq |g|\sqrt{10}. \tag{2.25}$$

2.3.3 *Upscaling via volume averaging*

In this section, we present results of Battiato et al. (2009) for the upscaling of the third equation in Eq. (2.20). The remaining two equations in Eq. (2.20) are upscaled in a similar fashion. Details of the derivation can be found in Battiato et al. (2009).

We assume that reactions in the fluid phase are much faster than precipitation on the solid phase, so that $\langle \partial c_3/\partial t\rangle = \partial\langle c_3\rangle/\partial t$. No assumptions are required for the upscaling of the linear term $\langle Kc_3\rangle_B = K\langle c_3\rangle_B$. The averaging procedure is presented below as a series of propositions. Their proofs are provided in Battiato et al. (2009).

Proposition 2.3.1. *Suppose that the following scale constraints hold:*

1) $l \ll r_0$,
2) $r_0^2 \ll \overline{L}^2$ *where* $\overline{L} = min\{L_{c1}, L_\phi\}$,
3) $\epsilon \ll 1$ *where* $\epsilon = l/L_c$,
4) $r_0 \ll L_c$,
5) $r_0^2 \ll L_c L_{c1}$.

Then the average of the Laplacian in Eq. (2.20) *can be approximated by:*

$$\langle \hat{\nabla}^2 c_3\rangle = \phi\hat{\nabla}^2\langle c_3\rangle_B + \hat{\nabla}\phi\cdot\hat{\nabla}\langle c_3\rangle_B + \frac{1}{|\mathscr{V}|}\hat{\nabla}\cdot\int_{A_{ls}} \tilde{c}_3\mathbf{n}_{ls}\,\mathrm{d}A - a_v\,Da_{ls}\frac{\langle c_3\rangle_B - 1}{l} \tag{2.26}$$

where $a_v \equiv |\mathscr{A}_{ls}|/|\mathscr{V}|$ *and* $\tilde{c}_3$ *is such that* $c_3 = \langle c_3\rangle_B + \tilde{c}_3$.

Proposition 2.3.2. *Suppose that the scale constraints 3)–5) of the Proposition 2.3.1 hold. Then the average of the reaction term in Eq.* (2.20) *can be approximated by:*

$$\langle c_1 c_2\rangle = \phi\,\langle c_1\rangle_B\,\langle c_2\rangle_B\,. \tag{2.27}$$

Proposition 2.3.3. *Suppose that in addition to the constraints in Proposition 2.3.1 the following scale constraints hold:*

1) $a_v \approx l^{-1}$,
2) $t \gg Da$,
3) $l \ll L_\phi$.

Then, the concentration fluctuations $\tilde{c}_3$ *satisfy a differential equation:*

$$0 = \frac{ql^2}{Da}\hat{\nabla}^2\tilde{c}_3 + \frac{qa_v l}{\phi}\frac{Da_{ls}}{Da}(\langle c_3\rangle_B - 1) + \tilde{c}_1\langle c_2\rangle_B + \tilde{c}_2\,\langle c_1\rangle_B + \tilde{c}_1\tilde{c}_2 - K\tilde{c}_3 \tag{2.28}$$

subject to the boundary conditions:

$$-\mathbf{n}\cdot\hat{\nabla}\tilde{c}_3 = \mathbf{n}\cdot\hat{\nabla}\langle c_3\rangle_B + Da_{ls}\frac{\langle c_3\rangle_B + \tilde{c}_3 - 1}{l}. \tag{2.29}$$

Boundary-value problems for fluctuations $\tilde{c}_1$ and $\tilde{c}_2$ are derived in a similar manner. Further progress requires an assumption of periodicity of the porous medium.

Proposition 2.3.4. *Suppose that in addition to the scale constraints imposed by Propositions 2.3.1 and 2.3.3 the porous medium is periodic with a unit cell characterized by* $\mathbf{n}(\hat{\mathbf{r}}+\hat{\mathbf{l}}_i)=\mathbf{n}(\hat{\mathbf{r}})$*, where* $\hat{\mathbf{l}}_i$ *with* $i=1,2,3$ *represents the three lattice vectors describing a spatially periodic porous medium. Then concentration fluctuations are periodic,* $\tilde{c}(\hat{\mathbf{r}}+\hat{\mathbf{l}}_i)=\tilde{c}(\hat{\mathbf{r}})$*, and* $\langle c_3\rangle_B$ *and* $\hat{\nabla}\langle c_3\rangle_B$ *in Eqs.* (2.28) *and* (2.29) *are evaluated at the centroid.*

Proposition 2.3.5. *Suppose that in addition to the constraint imposed by Proposition 2.3.3 the following constraints hold:*

1) $Da_{ls}\ll\epsilon$.
2) $Da\ll 1$,

Then concentration fluctuations $\tilde{c}_3$ *can be represented in terms of the macroscopic variables as:*

$$\tilde{c}_3=\hat{\mathbf{b}}\cdot\hat{\nabla}\langle c_3\rangle_B+s\langle c_3\rangle_B+\psi, \tag{2.30}$$

where the closure variables $\hat{\mathbf{b}}$*,* s *and* ψ *are solutions of the boundary value problems (wherein* $j=1,2,3$*):*

$$\hat{\nabla}^2\hat{\mathbf{b}}-\frac{k_3}{\mathscr{D}}\hat{\mathbf{b}}=\mathbf{0},\qquad -\mathbf{n}\cdot\hat{\nabla}\hat{\mathbf{b}}=\mathbf{n}\quad at\ A_{ls},\qquad \hat{\mathbf{b}}(\hat{\mathbf{r}}+\hat{\mathbf{l}}_j)=\hat{\mathbf{b}}(\hat{\mathbf{r}}) \tag{2.31}$$

$$\hat{\nabla}^2 s-\frac{k_3}{\mathscr{D}}s=-\frac{a_v Da_{ls}}{\phi l},\qquad -\mathbf{n}\cdot\hat{\nabla}s=\frac{Da_{ls}}{l}\langle c_3\rangle^l\quad at\ A_{ls},\qquad s(\hat{\mathbf{r}}+\hat{\mathbf{l}}_j)=s(\hat{\mathbf{r}}); \tag{2.32}$$

$$\hat{\nabla}^2\psi-\frac{k_3}{\mathscr{D}}\psi=\frac{a_v Da_{ls}}{\phi l},\qquad -\mathbf{n}\cdot\hat{\nabla}\psi=-\frac{Da_{ls}}{l}\quad at\ A_{ls},\qquad \psi(\hat{\mathbf{r}}+\hat{\mathbf{l}}_j)=\psi(\hat{\mathbf{r}}). \tag{2.33}$$

Combining the results from Propositions 2.3.1–2.3.5 with analogous results for $\langle c_1\rangle_B$ and $\langle c_2\rangle_B$, the volume averaging of Eq. (2.20) leads to a system of macroscopic equations:

$$\phi\frac{\partial\langle c_i\rangle_B}{\partial t}=\frac{\epsilon^2}{Da}\nabla\cdot(\phi\mathbf{D}_{\text{eff}}\cdot\nabla\langle c_i\rangle_B)-\phi\langle c_1\rangle_B\langle c_2\rangle_B+\phi K\langle c_3\rangle_B\qquad (i=1,2), \tag{2.34}$$

$$\phi q\frac{\partial\langle c_3\rangle_B}{\partial t}=\frac{q\epsilon^2}{Da}\nabla\cdot(\phi\mathbf{D}_{\text{eff}}\cdot\nabla\langle c_3\rangle_B)-qa_v l\frac{Da_{ls}}{Da}[\langle c_3\rangle_B-1]+\phi\langle c_1\rangle_B\langle c_2\rangle_B-\phi K\langle c_3\rangle_B, \tag{2.35}$$

where the effective diffusivity tensor $\mathbf{D}_{\text{eff}}$ is defined as:

$$\mathbf{D}_{\text{eff}}=\mathbf{I}+\frac{1}{|B|}\int_{A_{ls}}\mathbf{n}\hat{\mathbf{b}}\,\mathrm{d}A. \tag{2.36}$$

According to Proposition 2.3.5, a sufficient condition for the validity of the macroscopic description Eqs. (2.34)–(2.35), requires that $Da\ll 1$, which implies that on the pore scale the system is well-mixed with diffusion dominating reactions. Further insight is gained by relating different macroscopic diffusion and/or reaction regimes to the Damköhler number Da expressed in terms of the scale-separation parameter ϵ. (This is conceptually similar to the Auriault and Adler (1995) analysis of macroscopic dispersion equations, which identifies distinct transport regimes by expressing the Péclet number as powers of ϵ.) Interplay between the Damköhler number and ϵ determines whether macroscopic RDEs, Eqs. (2.34) and (2.35), are diffusion or reaction dominated. For $Da<\epsilon^2$, the macroscopic process is diffusion-driven and the nonlinear effects introduced by reactions are negligible. The two mechanisms are of the same order of magnitude in the region $\epsilon^2<Da<\epsilon$, and reactions dominate diffusion if $\epsilon<Da<1$. Mixing-induced precipitation, which is characterized by $Da\gg 1$, falls into the category of physical phenomena for which pore-scale or hybrid simulations are a priori necessary.

2.3.4 *Advection-diffusion-reaction equation*

Consider reactive transport in a porous medium whose characteristic length is L. Let us assume that the medium can be represented microscopically by a collection of spatially periodic "unit cells" with a characteristic length l, such that a scale parameter $\varepsilon \equiv l/L \ll 1$. Spatially periodic representations of micro-structures of porous media are routinely used to derive macroscopic properties and effective models of phenomena taking place in disordered media that lack such periodicity (Nitsche & Brenner 1989, Section 2). The unit cell $\hat{\mathcal{Y}} = \hat{B} \cup \hat{G}$ consists of the pore space $\hat{B}$ and the impermeable solid matrix $\hat{G}$ that are separated by the smooth surface $\hat{A}_{ls}$. The pore spaces $\hat{B}$ of each cell $\hat{\mathcal{Y}}$ form a multi-connected pore-space domain $\hat{B}^\varepsilon \subset \hat{\Omega}$ bounded by the smooth surface $\hat{A}^\varepsilon_{ls}$.

2.3.4.1 *Governing equations*

Single-phase flow of an incompressible fluid in the pore-space $\hat{B}^\varepsilon$ is described by the Stokes and continuity equations Eq. (2.8) subject to the no-slip boundary condition on $\hat{A}^\varepsilon_{ls}$. The fluid contains a dissolved species $\mathcal{M}$, whose molar concentration $\hat{c}_\varepsilon(\hat{\mathbf{x}}, \hat{t})$ $[molL^{-3}]$ at point $\hat{\mathbf{x}} \in \hat{B}^\varepsilon$ and time $\hat{t} > 0$ changes due to advection, molecular diffusion, and a nonlinear heterogeneous reaction at the solid-liquid interface $\hat{A}^\varepsilon_{ls}$. The first two phenomena are described by the advection-diffusion equation Eq. (2.12).

Whenever the concentration $\hat{c}_\varepsilon$ exceeds a threshold value $\overline{c}$, a heterogeneous reaction $n\mathcal{M} \leftrightarrow \mathcal{N}_{(s)}$ occurs, in which n molecules of the solute $\mathcal{M}$ precipitate in the form of one molecule of a crystalline solid $\mathcal{N}_{(s)}$. At the solid-liquid interface $\hat{A}^\varepsilon_{ls}$ impermeable to flow, mass conservation requires that mass flux of the species $\mathcal{M}$ be balanced by the difference between the precipitation rate R_p and the dissolution rate R_d:

$$-\mathbf{n} \cdot \hat{\mathbf{D}} \hat{\nabla} \hat{c}_\varepsilon = R_p - R_d, \tag{2.37}$$

where $\mathbf{n}$ is the outward unit normal vector of $\hat{A}^\varepsilon_{ls}$. Following Knabner et al. (1995), we assume that $R_p = \hat{k}\hat{c}^a_\varepsilon$ and $R_d = \hat{k}\overline{c}^a$, where $\hat{k}$ $[L^{3a-2}T^{-1}mol^{1-a}]$ is the reaction rate constant, $a \in \mathbf{Z}^+$ is related to the order of reaction n (Morse & Arvidson 2002, Eq. 6), and the threshold concentration $\overline{c}$ represents the solubility product (Morse & Arvidson 2002). Mass conservation on the liquid-solid interface $\hat{A}^\varepsilon_{ls}$ yields a boundary condition (Morse & Arvidson 2002, Eq. 5):

$$-\mathbf{n} \cdot \hat{\mathbf{D}} \hat{\nabla} \hat{c}_\varepsilon = \hat{k}(\hat{c}^a_\varepsilon - \overline{c}^a), \qquad \hat{\mathbf{x}} \in \hat{A}^\varepsilon_{ls}, \qquad \hat{t} > 0. \tag{2.38}$$

In addition to Eq. (2.38), the flow and transport equations Eq. (2.8) and Eq. (2.12) are supplemented with proper boundary conditions on the external boundary of the flow domain $\hat{\Omega}$.

2.3.4.2 *Dimensionless formulation*

Let us introduce dimensionless quantities:

$$c_\varepsilon = \hat{c}_\varepsilon/\overline{c}, \quad \mathbf{x} = \hat{\mathbf{x}}/L, \quad \mathbf{v}_\varepsilon = \hat{\mathbf{v}}_\varepsilon/U, \quad \mathbf{D} = \hat{\mathbf{D}}/D, \quad p = \hat{p}l^2/\hat{\mu}UL, \tag{2.39}$$

where D and U are characteristic values of $\mathbf{D}$ and $\mathbf{v}_\varepsilon$, respectively. The scaling of pressure $\hat{p}$ ensures that the pressure gradient and the viscous term are of the same order of magnitude, as prescribed by Stokes equation (Auriault & Adler 1995, Eqs. 15 and 16). Furthermore, we define three time scales associated with diffusion ($\hat{t}_D$), reactions ($\hat{t}_R$) and advection ($\hat{t}_A$) as:

$$\hat{t}_D = \frac{L^2}{D}, \qquad \hat{t}_R = \frac{L}{\hat{k}\overline{c}^{a-1}}, \qquad \hat{t}_A = \frac{L}{U}. \tag{2.40}$$

Ratios between these time scales define the dimensionless Damköhler ($Da = \hat{t}_D/\hat{t}_R$) and Péclet ($Pe = \hat{t}_D/\hat{t}_A$) numbers:

$$Da = \frac{L\hat{k}\overline{c}^{a-1}}{D} \quad \text{and} \quad Pe = \frac{UL}{D}. \tag{2.41}$$

Rewriting Eqs. (2.8), (2.12) and (2.38) in terms of the dimensionless quantities Eq. (2.39) and the dimensionless time $t = \hat{t}/\hat{t}_D$ yields a dimensionless form of the flow equations:

$$\varepsilon^2 \nabla^2 \mathbf{v}_\varepsilon - \nabla p = 0, \qquad \nabla \cdot \mathbf{v}_\varepsilon = 0, \qquad \mathbf{x} \in B^\varepsilon, \tag{2.42}$$

subject to:

$$\mathbf{v}_\varepsilon = \mathbf{0}, \qquad \mathbf{x} \in A_{ls}^\varepsilon \tag{2.43}$$

and a dimensionless form of the transport equation:

$$\frac{\partial c_\varepsilon}{\partial t} + \nabla \cdot (-\mathbf{D}\nabla c_\varepsilon + \mathrm{Pe}\mathbf{v}_\varepsilon c_\varepsilon) = 0, \qquad \mathbf{x} \in B^\varepsilon, \qquad t > 0, \tag{2.44}$$

subject to:

$$-\mathbf{n} \cdot \mathbf{D}\nabla c_\varepsilon = \mathrm{Da}(c_\varepsilon^a - 1), \qquad \mathbf{x} \in A_{ls}^\varepsilon, \qquad t > 0. \tag{2.45}$$

2.3.4.3 *Homogenization via multiple-scale expansions*

Homogenization aims to derive effective equations for average state variables that are representative of an averaging volume (e.g., Darcy scale). To this end, two types of local averages of a quantity $c(\mathbf{x})$ can be defined as in Eq. (2.23). We also define:

$$\langle \mathcal{A} \rangle_{ls} \equiv \frac{1}{|A_{ls}|} \int_{A_{ls}(\mathbf{x})} \mathcal{A}\, \mathrm{d}\mathbf{y}. \tag{2.46}$$

In the subsequent derivation of effective (continuum- or Darcy-scale) equations for average flow velocity $\langle \mathbf{v}(\mathbf{x}) \rangle$ and solute concentration $\langle c(\mathbf{x}, t) \rangle$, we employ the method of multiple-scale expansions (Auriault & Adler 1995, Hornung 1997).

The method of multiple-scale expansions introduces a fast space variable $\mathbf{y}$ and two time variables τ_r and τ_a:

$$\mathbf{y} = \frac{\mathbf{x}}{\varepsilon}, \qquad \tau_r = Da\, t = \frac{\hat{t}}{\hat{t}_R}, \qquad \tau_a = Pe\, t = \frac{\hat{t}}{\hat{t}_A}. \tag{2.47}$$

Furthermore, it represents the concentration $c_\varepsilon(\mathbf{x}, t)$ in Eq. (2.44) as $c_\varepsilon(\mathbf{x}, t) := c(\mathbf{x}, \mathbf{y}, t, \tau_r, \tau_a)$. The latter is expanded into an asymptotic series in powers of ε:

$$c(\mathbf{x}, \mathbf{y}, t, \tau_r, \tau_a) = \sum_{m=0}^{\infty} \varepsilon^m c_m(\mathbf{x}, \mathbf{y}, t, \tau_r, \tau_a), \tag{2.48}$$

wherein $c_m(\mathbf{x}, \mathbf{y}, t, \tau_r, \tau_a)$ $(m = 0, 1, \ldots)$ are $\mathcal{V}$-periodic in $\mathbf{y}$. Finally, we set:

$$Pe = \varepsilon^{-\alpha} \quad \text{and} \quad Da = \varepsilon^\beta, \tag{2.49}$$

with the exponents α and β determining the system behavior. For example, transport due to advection and dispersion at the pore scale is not homogenizable if $\alpha \geq 2$ (Auriault & Adler 1995, Section 3.5, Table 1).

Pore-scale reactive transport processes described by Eqs. (2.44)–(2.45) can be homogenized, i.e., approximated up to order ε^2 with an effective ADRE:

$$\phi \frac{\partial \langle c \rangle_B}{\partial t} = \nabla \cdot (\mathbf{D}^* \nabla \langle c \rangle_B - Pe \langle c \rangle_B \langle \mathbf{v} \rangle) - \varepsilon^{-1} \phi Da \mathcal{K}^* (\langle c \rangle_B^a - 1), \quad \mathbf{x} \in \Omega, \tag{2.50}$$

provided the following conditions are met:

1) $\varepsilon \ll 1$,
2) $Pe < \varepsilon^{-2}$,
3) $Da/Pe < \varepsilon$,

4) $Da < 1$,
5) $\langle \boldsymbol{\chi} \rangle_{ls} \approx \langle \boldsymbol{\chi} \rangle_B$.

In Eq. (2.50), the dimensionless effective reaction rate constant $\mathscr{K}^*$ is determined by the pore geometry:

$$\mathscr{K}^* = \frac{|A_{ls}|}{|B|}, \tag{2.51}$$

and the dispersion tensor $\mathbf{D}^*$ is given by:

$$\mathbf{D}^* = \langle \mathbf{D}(\mathbf{I} + \nabla_{\mathbf{y}} \boldsymbol{\chi}) \rangle + \varepsilon \, Pe \langle \boldsymbol{\chi} \mathbf{k} \rangle \nabla_{\mathbf{x}} p_0. \tag{2.52}$$

The closure variable $\boldsymbol{\chi}(\mathbf{y})$ has zero mean, $\langle \boldsymbol{\chi} \rangle = \mathbf{0}$, and is defined as a solution of the local problem:

$$-\nabla_{\mathbf{y}} \cdot \mathbf{D}(\nabla_{\mathbf{y}} \boldsymbol{\chi} + \mathbf{I}) + \varepsilon \, Pe \, \mathbf{v}_0 \nabla_{\mathbf{y}} \boldsymbol{\chi} = \varepsilon \, Pe \, (\langle \mathbf{v}_0 \rangle_B - \mathbf{v}_0), \qquad \mathbf{y} \in B; \tag{2.53a}$$

$$-\mathbf{n} \cdot \mathbf{D}(\nabla_{\mathbf{y}} \boldsymbol{\chi} + \mathbf{I}) = 0, \qquad \mathbf{y} \in A_{ls}; \tag{2.53b}$$

where $\mathbf{v}_0 = -\mathbf{k} \cdot \nabla_{\mathbf{x}} p_0$ and the pressure p_0 is a solution of:

$$\langle \mathbf{v} \rangle = -\mathbf{K} \cdot \nabla p_0, \qquad \nabla \cdot \langle \mathbf{v} \rangle = 0, \qquad \mathbf{x} \in \Omega. \tag{2.54}$$

Details of the derivations can be found in Battiato and Tartakovsky (2010). Constraints 1)–4) ensure the separation of scales. While constraint 1) is almost always met in practical applications, the rest of them depend on the relative importance of advective, diffusive, and reactive mechanisms of transport. These conditions are summarized in the phase diagram in Fig. 2.1, where the line $\beta = 0$ refers to $Da = 1$ and the half-space $\beta > 0$ to $Da < 1$ because $\varepsilon < 1$; the line $\alpha = 2$ refers to $Pe = \varepsilon^{-2}$ and the half-space $\alpha < 2$ refers to $Pe < \varepsilon^{-2}$; the line $\alpha + \beta = 1$ refers to $Da/Pe = \varepsilon$; and the half-space underneath this line refers to $Da/Pe < \varepsilon$. Constraints 3) and 4) require that either diffusion or advection-diffusion dominate reactions at the pore scale. This allows one to decouple the pore- and continuum-scale descriptions. Constraint 5) is not required for scale separation, but facilitates the derivation of the effective parameters Eq. (2.51) and Eq. (2.52). This constraint allows one to interchange the surface and volume averages, $\langle c_1 \rangle_{ls} \approx \langle c_1 \rangle_B$, within errors on the order of ε^2.

The results above generalize the conclusions of the analysis of reactive-diffusive transport performed in Section 2.3.1, which relied on the method of volume averaging. While using different upscaling approaches, both analyses provide the same bound on the Damköhler number Da in the absence of advection. The effective reaction rate $\mathscr{K}^*$ for heterogeneous reactions Eq. (2.51) is likewise consistent with that obtained by Battiato et al. (2009). This suggests that the conditions for validity and breakdown of continuum models of reactive transport presented in the phase diagram in Fig. 2.1 are universal and independent of the upscaling method. Finally, these upscaling results justify the use of reaction terms similar to the one in Eq. (2.50) in continuum models of precipitation and dissolution processes in porous media (Lichtner & Tartakovsky 2003, Tartakovsky et al. 2009, Broyda et al. 2010).

2.4 HYBRID MODELS FOR TRANSPORT IN POROUS MEDIA

2.4.1 *Intrusive hybrid algorithm*

Having identified the criteria of the applicability of macroscopic equations, we present a hybrid algorithm that couples pore-scale simulations in a small domain Ω_p with continuum simulations elsewhere in the computational domain, Ω / Ω_p. The coupling is accomplished via an iterative procedure in a handshake region Ω_{pc}, where both pore-scale and continuum-scale descriptions are solved iteratively to ensure the continuity of state variables and their fluxes across the interface between Ω_p and the rest of the computational domain.

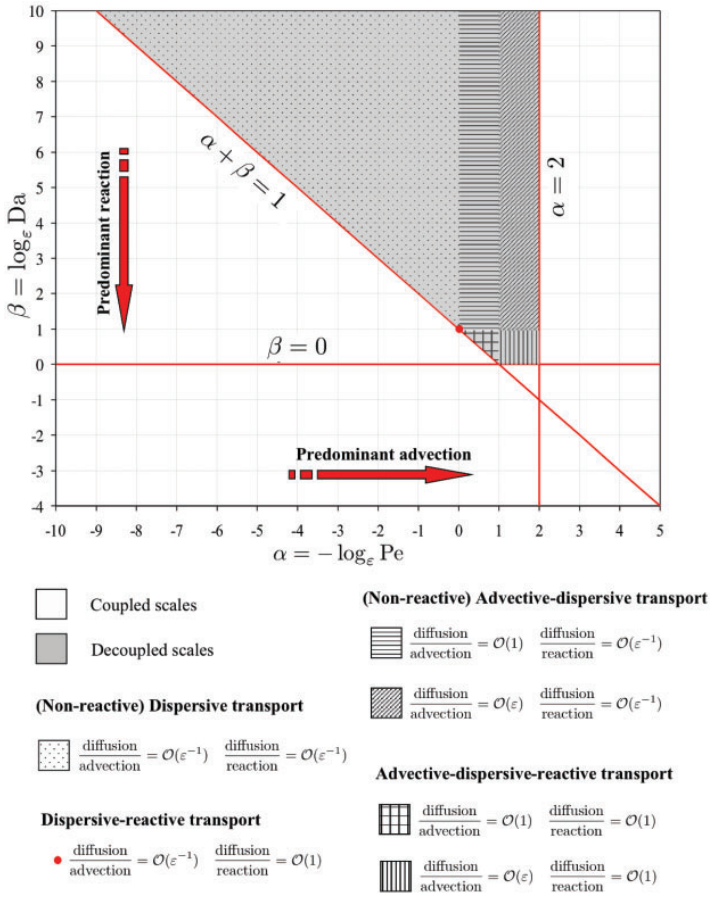

Figure 2.1 Phase diagram indicating the range of applicability of macroscopic equations for the advection-reaction-diffusion system Eqs. (2.44)–(2.45), in terms of *Pe* and *Da*. The grey region identifies the sufficient conditions under which the macroscopic equations hold. In the white region, macro- and micro-scale problems are coupled and have to be solved simultaneously. Also identified are different transport regimes depending on the order of magnitude of *Pe* and *Da*. Diffusion, advection, and reaction are of the same order of magnitude at the point $(\alpha, \beta) = (1, 0)$. After Battiato and Tartakovsky (2010).

This section contains a general formulation of flow and transport equations at the pore- and continuum-scales (Section 4.1.1), as well as an outline of the proposed hybrid algorithm (Section 2.4.1.2). Both the hybrid formulation and its numerical implementation are demonstrated in Section 2.4.2 by applying them to model Taylor dispersion in a planar fracture with chemically reactive walls. In Section 2.4.4, we use this well-studied problem to validate our hybrid algorithm via comparison with analytical solutions and two-dimensional pore-scale numerical simulations.

2.4.1.1 *Governing equations at the pore- and continuum-scale*

Consider reactive transport in a fully-saturated porous medium Ω^T. Within the pore space Ω_l contained in Ω^T, single-phase flow of an incompressible fluid is described by the Stokes and continuity equations Eq. (2.8), subject to the no-slip boundary condition on the solid-liquid interface. The flow is driven by boundary conditions imposed on $\partial\Omega^T$, the external boundary of Ω^T.

The fluid contains a dissolved species with molar concentration $c(\mathbf{x}, t)$ $[ML^{-3}]$ that undergoes advection, molecular diffusion and a linear heterogeneous reaction at the solid-liquid interface A_{sl}. The evolution of $c(\mathbf{x}, t)$ is described by an advection-diffusion equation Eq. (2.12) with $\mathbf{D} = \mathscr{D}\mathbf{I}$ and $R(c) = 0$, subject to the boundary condition Eq. (2.13) on the solid-fluid interface with $Q(c) = \mathscr{K}c$. Proper boundary conditions are applied on the external boundary $\partial\Omega^T$. This leads to:

$$\frac{\partial c}{\partial t} + \nabla \cdot (\mathbf{v}c) = \mathscr{D}\nabla^2 c, \tag{2.55a}$$

subject to:

$$-\mathbf{n} \cdot \mathscr{D}\nabla c = \mathscr{K}c. \tag{2.55b}$$

where $\mathscr{D}$ $[L^2T^{-1}]$ is the molecular diffusion coefficient, $\mathscr{K}$ $[LT^{-1}]$ is the reaction constant describing an interface reaction (e.g., linear microbial degradation), and $\mathbf{n}$ is the outward unit normal vector of A_{sl}.

Let $\overline{A}(\mathbf{x}, t)$ denote the volumetric average of a pore-scale quantity $A(\mathbf{x}, t)$ defined as:

$$\overline{\mathcal{A}}(\mathbf{x}, t) \equiv \frac{1}{\phi|\mathscr{V}|} \int\limits_{\mathscr{V}(\mathbf{x})} \mathcal{A}(\mathbf{y}, t)\, \mathrm{d}\mathbf{y}, \tag{2.56}$$

where ϕ is the porosity of a porous medium and the averaging volume $\mathscr{V}$ might or might not constitute a representative elementary volume (REV).

The upscaling of Eq. (2.55) by standard upscaling methodologies e.g., multiple-scale expansions or volumetric averaging (e.g., Battiato & Tartakovsky 2010, and references therein), leads to:

$$\phi\frac{\partial \overline{c}}{\partial t} + \phi\nabla \cdot (\mathbf{V}\overline{c}) = \nabla \cdot (\mathbf{D}^*\nabla\overline{c}) - K\overline{c}, \tag{2.57}$$

where $\mathbf{D}^*$ is the dispersion tensor, $\mathbf{V} = \phi\overline{\mathbf{v}}$ is Darcy's flux (Auriault & Adler 1995) and K is the effective reaction rate. As previously discussed, a number of simplifying approximations are required for Eq. (2.57) to be valid regardless of the choice of an upscaling technique.

2.4.1.2 *General hybrid formulation*

When Darcy's law is valid over the whole computational domain Ω^T but one or more of the sufficient conditions (Battiato and Tartakovsky 2010, Battiato et al. 2009) for the validity of the continuum-scale transport equation Eq. (2.57) break down in a sub-domain Ω_p of the computational domain Ω (Fig. 2.2), the averaging in Ω_p of Eq. (2.55) results in an integro-differential equation:

$$\phi\frac{\mathrm{d}\overline{c}}{\mathrm{d}t} + \overline{\nabla \cdot (\mathbf{v}c)} = \mathscr{D}\overline{\nabla^2 c}. \tag{2.58}$$

Here the averaging of Eq. (2.56) is defined over $\mathscr{V} \equiv \Omega_p(\mathbf{x}^\star)$ and $\mathbf{x}^\star$ is the centroid of Ω_p, i.e., the subdomain Ω_p shrinks to a point $\mathbf{x}^\star \in \Omega^T$.

Application of Gauss' theorem, boundary condition Eq. (2.55b) and the no-slip condition yield:

$$\phi\frac{\partial \overline{c}}{\partial t} = -\frac{1}{\phi|\Omega_p|} \int\limits_{A_{ll}^p} q_n\, \mathrm{d}s - \frac{1}{\phi|\Omega_p|} \int\limits_{A_{sl}^p} \mathscr{K}c\, \mathrm{d}s, \tag{2.59}$$

where $A_p = A_{ll}^p \cup A_{sl}^p$ is the bounding surface of Ω_p and consists of liquid-liquid (A_{ll}^p) and solid-liquid (A_{sl}^p) segments, $\mathrm{d}s$ is an infinitesimal element of A_p and $q_n = \mathbf{n} \cdot (\mathbf{v}c - \mathscr{D}\nabla c)$ is the flux through the liquid-liquid portion of the boundary, A_p. The right hand side of Eq. (2.59) depends on pore-scale quantities. It represents the fluxes exchanged at the boundary A_p between the pore- and continuum-scale descriptions. While multiscale approaches (Christie 1996, Efendiev & Durlofsky 2003, Langlo & Espedal 1994, among others) aim to decouple the two descriptions by employing closure assumptions for the the unresolved flux, q_n, our goal is to preserve the nonlinearity of the

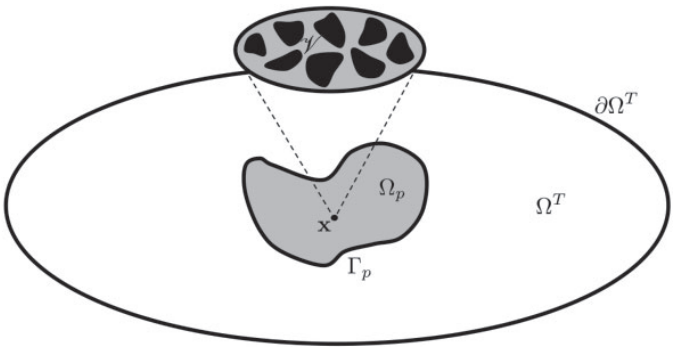

Figure 2.2 A schematic representation of the pore- and continuum-scale domains. After Battiato et al. (2010).

problem and to compute the unresolved normal flux q_n without any assumption on the microscale behavior.

This will allow us to bypass the assumptions needed for continuum-scale models. To this end, we obtain the pore-scale concentration $c(\mathbf{x}, t)$ in Eq. (2.59) by solving the transport problem Eq. (2.55) defined on Ω_p. The boundary condition Eq. (2.55b) is now defined on the union of all solid-liquid surfaces A_{sl} contained in Ω_p. On the fluid-fluid segments A_{ll}^p, mass conservation requires that $\mathbf{n} \cdot (\mathscr{D}\nabla c - \mathbf{v}c) = q_n$. The flux q_n, which represents a boundary condition for the pore-scale problem Eq. (2.55) and a source term for the continuum-scale equation Eq. (2.59), is unknown.

In summary, the hybrid pore-scale/continuum scale algorithm contains the three unknowns $(c, \overline{c}, q_n)$ that satisfy a system of coupled partial-differential equations (Battiato et al. 2010):

$$\phi\frac{\partial \overline{c}}{\partial t} + \phi\nabla\cdot(\mathbf{V}\overline{c}) = \nabla\cdot(\mathbf{D}\nabla\overline{c}) - K\overline{c}, \quad \mathbf{x}\in\Omega^T, \quad t>0 \tag{2.60}$$

$$\phi\frac{\mathrm{d}\overline{c}}{\mathrm{d}t} = \frac{1}{\phi|\Omega_p|}\int_{A_{ll}} q_n\,\mathrm{d}\mathbf{x} - \frac{1}{\phi|\Omega_p|}\int_{A_{sl}} \mathscr{K}c\,\mathrm{d}\mathbf{x}, \quad \mathbf{x}=\mathbf{x}^\star, \quad t>0 \tag{2.61}$$

$$\frac{\partial c}{\partial t} + \nabla\cdot(\mathbf{v}c) = \mathscr{D}\nabla^2 c, \qquad \mathbf{x}\in\Omega_p, \quad t>0 \tag{2.62}$$

$$\mathbf{n}\cdot(\mathscr{D}\nabla c - \mathbf{v}c) = q_n, \qquad \mathbf{x}\in A_{ll}, \quad t>0 \tag{2.63}$$

$$-\mathbf{n}\cdot\mathscr{D}\nabla c = \mathscr{K}c, \qquad \mathbf{x}\in A_{sl}, \quad t>0, \tag{2.64}$$

supplemented by boundary conditions on the external domain $\partial\Omega^T$ and initial conditions.

2.4.2 *Taylor dispersion in a fracture with reactive walls*

Transport of a reactive solute by advection and diffusion in a fracture of width $2H$ that undergoes a first-order heterogeneous reaction at the walls of the channel is described by:

$$\frac{\partial c}{\partial t} + u(y)\frac{\partial c}{\partial x} - \mathscr{D}\left(\frac{\partial^2 c}{\partial x^2} + \frac{\partial^2 c}{\partial y^2}\right) = 0, \qquad (x,y)\in\Omega, \quad t>0 \tag{2.65a}$$

$$-\mathscr{D}\frac{\partial c}{\partial y} = \mathscr{K}c, \qquad (x,y)\in A, \quad t>0, \tag{2.65b}$$

where the flow domain $\Omega = \{(x,y) : x\in(0,\infty), |y|<H\}$ has the boundary $A = \{(x,y) : x\in(0,\infty), |y|=H\}$. A fully developed flow assumption in laminar regime yields to a Poiseuille's velocity profile for the pore-scale velocity $\mathbf{v} = (u,0)^T$, $u(y) = u_m[1-(y/H)^2]$, where u_m is the maximum

velocity at the center of the fracture ($y = 0$). The average concentration $\overline{c}(x,t)$ in Eq. (2.56) is now defined as:

$$\overline{c}(x,t) \equiv \frac{1}{2H}\int_{-H}^{H} c(x,y,t)\,\mathrm{d}y. \tag{2.66}$$

It satisfies the Darcy-scale equation (Mikelić et al. 2006):

$$\frac{\partial \overline{c}}{\partial t} + U\frac{\partial \overline{c}}{\partial x} + K\overline{c} = D\frac{\partial^2 \overline{c}}{\partial x^2}, \qquad x \in (0,\infty), \quad t > 0, \tag{2.67a}$$

where

$$U = u_m\left(\frac{2}{3} + \frac{4\mathrm{Da}_y}{45}\right), \quad K = \frac{\mathscr{K}}{H}\left(1 - \frac{\mathrm{Da}_y}{3}\right), \quad D = \mathscr{D}\left(1 + \frac{8\mathrm{Pe}_y^2}{945}\right) \tag{2.67b}$$

and

$$\mathrm{Pe}_y = \frac{u_m H}{\mathscr{D}}, \qquad \mathrm{Da}_y = \frac{\mathscr{K} H}{\mathscr{D}}. \tag{2.67c}$$

The validity of Eq. (2.67) requires that L, a macroscopic characteristic length scale in the x direction, be much larger than H, i.e., $\epsilon = H/L \ll 1$; and places a number of constraints on the order of magnitude of Pe and Da (see the phase diagram in Battiato and Tartakovsky (2010)). Specifically, Eq. (2.67) fails for $\mathrm{Da}_y \geq 3$ as K changes sign for increasing positive values of $\mathscr{K}$ (i.e., increasing mass loss at the solid-liquid interface): this leads to the unphysical behavior of $K < 0$ (i.e., source) while mass is absorbed (degraded, etc) at the micro-scale (i.e., sink).

Whenever one or more of these constraints are violated in a small portion of the computational domain, Ω_p, Eq. (2.67) is no longer valid and its nonlocal counterpart Eq. (2.59) must be employed. For the problem under consideration, the latter takes the form:

$$\frac{\partial \overline{c}}{\partial t} = \mathscr{D}\frac{\partial^2 \overline{c}}{\partial x^2} - \frac{\mathscr{K} J_c}{2H} - \overline{u(y)\frac{\partial c}{\partial x}}, \qquad (x,y) \in \Omega_p \tag{2.68}$$

where $\Omega_p = \{(x,y) : x \in (a,b), |y| < H\}$ corresponds to a single macroscale grid block, $J_c = c(x,H) + c(x,-H)$, and the pore-scale concentration $c(x,y,t)$ satisfies Eq. (2.65). Equation (2.68) is subject to boundary conditions at the internal boundary $A_p = \{(x,y) : x = a,b;\ y \in (-H,H)\}$:

$$\mathbf{n}\cdot(\mathbf{v}c - \mathscr{D}\nabla c) = q_n. \tag{2.69}$$

2.4.3 *Hybrid algorithm*

Solving the nonlinear coupled system Eqs. (2.65)–(2.69) reduces to finding zero q_n of an algebraic equation in the form $F(q_n) = 0$, where q_n is the unknown flux at the boundary of Ω_p. The hybrid pore-scale/continuum-scale algorithm can be formulated as follows.

- Initialization. At timestep T^N, c^N and $\overline{c}(t = T^N)$ are known.
- Guess for fluxes. Make a guess for q_n. This imposes the Robin conditions Eq. (2.69) on A_p.
- Pore-scale evolution. The pore-scale problem Eq. (2.65) is evolved from T^N to T^{N+1}. The source term.
- Evaluation of volume and boundary integrals. J_c and the volume integral in the right hand side of Eq. (2.68) are evaluated.
- Continuum-scale evolution. The continuum-scale concentration $\overline{c}$ is evolved from T^N to T^{N+1} by solving Eq. (2.68) in Ω_p and Eq. (2.67) in the remainder of the computational domain.

- Continuum-scale fluxes computation. Continuum-scale flux $\tilde{q}_n$ at the interface A_p is evaluated by differentiation of continuum-scale solution.
- Convergence check and iteration. Select an acceptable tolerance ϵ. If $|\tilde{q}_n - q_n| > \epsilon$, refine the guess of q_n and go to the second step. If $|\tilde{q}_n - q_n| \leq \epsilon$, then the convergence is reached. March forward in time ($N := N + 1$) and go to the first step.

2.4.4 *Numerical results*

A finite volume implementation of the problem of reactive transport through a fracture is discussed in Battiato et al. (2010). Spatial discretization of Eqs. (2.67) and (2.68) leads to an algebraic system of equations of the form $Ax = b$ with some of the coefficients $a_{i,j} = [A]_{i,j}$ and b_i dependent on pore-scale quantities. While such formulation naturally arises from upscaling techniques, its intrusive nature renders it less computationally appealing: at each macroscopic timestep, A must be evaluated and inverted.

Some of the results discussed in Battiato et al. (2010) are reported here for completeness. These include a hybrid validation for advective-diffusive transport in a fracture with uniform reaction rates. This setting admits an analytical solution and, hence, is used to analyze the accuracy of the hybrid algorithm relative to that of its continuum (upscaled) counterpart (Section 2.4.4.1). In Section 2.4.4.2, the reaction coefficient is taken to be highly heterogeneous. For this situation, a comparison of the hybrid solution with both a solution of the upscaled equation Eq. (2.67) and an averaged solution of the fully two-dimensional problem ("pore-scale simulations") is presented.

2.4.4.1 *Hybrid validation*

The macroscopic problem Eq. (2.67), subject to the initial and boundary conditions:

$$\overline{c}(x,0) = 1, \qquad \overline{c}(0,t) = 0, \qquad \frac{\partial \overline{c}}{\partial x}(\infty, t) = 0, \tag{2.70}$$

admits the unique solution

$$\overline{c}(x,t) = \mathrm{e}^{-Kt}\left(1 - \frac{1}{\sqrt{\pi}}\mathrm{e}^{Ux/D}\int_{\frac{x+Ut}{2\sqrt{Dt}}}^{+\infty}\mathrm{e}^{-\eta^2}\mathrm{d}\eta + \frac{1}{\sqrt{\pi}}\int_{\frac{x-Ut}{2\sqrt{Dt}}}^{+\infty}\mathrm{e}^{-\eta^2}\mathrm{d}\eta\right). \tag{2.71}$$

Battiato et al. (2010) use this exact solution to verify the accuracy of both the hybrid solution and the numerical solution of the continuum problem Eq. (2.67) for advective-diffusive transport (Fig. 2.3) and advective-diffusive-reactive transport with uniform reaction rates (Fig. 2.4). The agreement between analytical and hybrid solution is perfect, which is to be expected since all the necessary conditions for the validity of the macroscopic (averaged) transport equation Eq. (2.67) hold for these flow and transport regimes. The parameter values used in these and subsequent simulations are provided in Battiato et al. (2010).

2.4.4.2 *Hybrid simulations for highly localized heterogeneous reaction*

Effects heterogenous reaction coefficient are presented. We allow $\mathscr{K}$ to change by two orders of magnitude with a typical Damköhler number ranging from 0.03 to 2.8. Specifically $\mathscr{K} = \mathscr{K}_{\text{in}}$ for $x = 3.75$ and $\mathscr{K} = \mathscr{K}_{\text{out}}$ everywhere else, with $\mathscr{K}_{\text{in}} = 450$ and $\mathscr{K}_{\text{out}} = 5$. We show here that significant deviations from the "pore-scale" solution occur even for $\text{Da} < 3$. The results of our hybrid simulations are compared with that of the upscaled 1D equation and the average of the fully 2D solution. Figure 2.5 shows the continuum-scale concentration obtained from the upscaled 1D continuum-scale, hybrid simulations and the 2D pore-scale equations. At the location of high heterogeneity, the continuum-scale equation overestimates the concentration, with values that double the true concentration obtained from the pore-scale simulations. On the contrary, the hybrid simulation significantly improves the predictions.

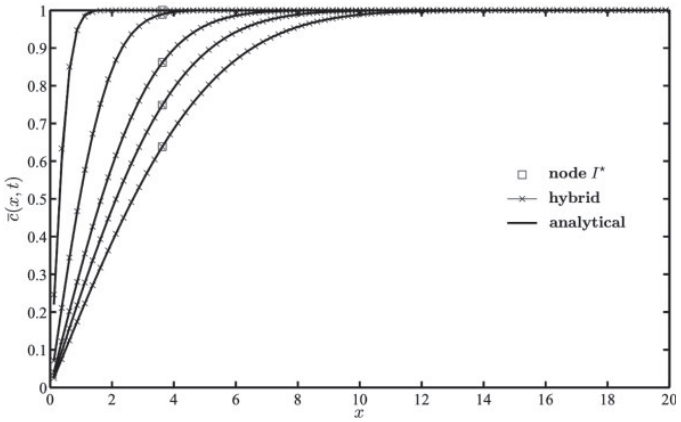

Figure 2.3 Advection-diffusion: Temporal snapshots of the average concentration $\overline{c}$ obtained analytically by Eq. (2.71) (solid line) and from hybrid simulation ($\times$) at times $t = 0.005$, $t = 0.05$, $t = 0.15$, $t = 0.25$, and $t = 0.395$ (from left to right). The box indicates the location where pore- and continuum-scales are coupled. After Battiato et al. (2010).

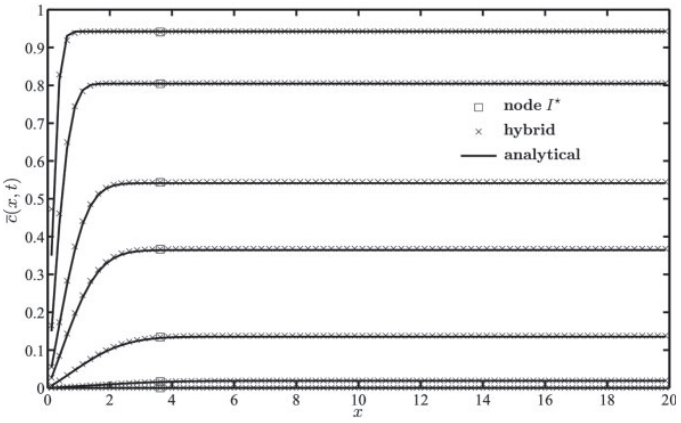

Figure 2.4 Advection-diffusion-reaction with homogeneous reaction rate: Temporal snapshots of the average concentration $\overline{c}$ obtained analytically by Eq. (2.71) (solid line) and from hybrid simulation ($\times$) at times $t = 0.001$, $t = 0.005$, $t = 0.015$, $t = 0.025$, $t = 0.05$, $t = 0.1$, and $t = 0.195$ (from top to bottom). The box indicates the location where pore- and continuum-scales are coupled. After Battiato et al. (2010).

2.4.5 *Non-intrusive hybrid algorithm*

Th hybrid algorithm developed in the previous section is intrusive in that it requires the modification of some of the coefficients of the system of discretized equations. Even though its formulation is quite general and can be applied to a variety of different numerical schemes, its implementation in legacy codes, in which discretized equations cannot be easily modified by the user, is challenging. Complex pore geometries introduce another complication.

Hence, a desirable feature of a hybrid algorithm is its portability and implementation in existing codes. This can be accomplished by eliminating the overlapping ("handshake") region and formulating appropriate conditions at the interfaces separating the two computational subdomains,

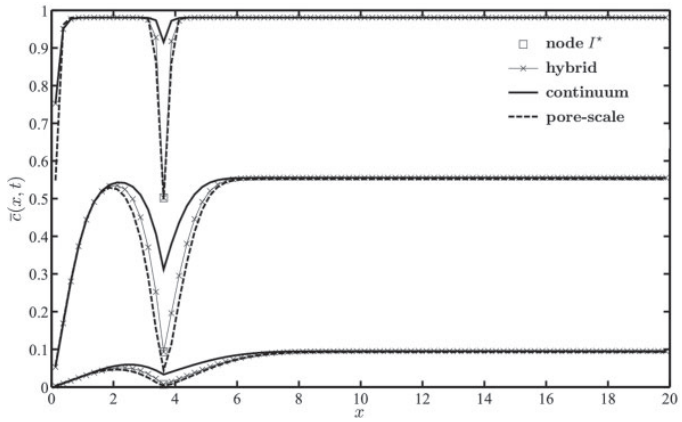

Figure 2.5 Advection-diffusion-reaction with localized reaction rate: Temporal snapshots of the average concentration $\overline{c}$ obtained from the 1D upscaled equation (solid line), from hybrid simulations ($-\times-$) and from the 2D pore-scale simulations (dashed line) at times $t = 0.0005$ (top), $t = 0.015$ (center) and $t = 0.06$ (bottom). The box indicates the location where pore- and continuum-scales are coupled. After Battiato et al. (2010).

while ensuring the continuity of state variables and fluxes. Within this framework, pore-scale simulations affect a continuum-scale solution through boundary conditions (and not as a modification of continuum-scale discretized equations): this will facilitate hybrid implementation for existing codes and/or software.

2.4.5.1 *Governing equations at the pore- and continuum-scale for advective-diffusive systems*
Consider advective-diffusive transport in a fully saturated porous medium Ω^T. Within the pore space $\Omega^T_{pore} \subset \Omega^T$, single-phase flow of an incompressible fluid is described by the Stokes and continuity equations Eq. (2.8). Flow equations are subject to the no-slip boundary condition on the solid-liquid interface $A^T_{s\ell}$, which is taken to be impermeable to flow. The flow is driven by boundary conditions imposed on $\partial\Omega^T$, the external boundary of Ω^T. The fluid contains a dissolved species with molar concentration $c(\mathbf{x}, t)$ that is advected and diffused in the system.

The evolution of the concentration $c(\mathbf{x}, t)$ of a tracer undergoing advection and diffusion is described by:

$$\frac{\partial c}{\partial t} + \nabla \cdot (\mathbf{v}c) = \mathscr{D}\nabla^2 c, \tag{2.72}$$

subject to a no-flux boundary condition on the solid-fluid interface $A^T_{s\ell}$

$$-\mathbf{n} \cdot \mathscr{D}\nabla c = 0, \tag{2.73}$$

and proper boundary conditions on $\partial\Omega^T$.

Let $\overline{A}(\mathbf{x}, t)$ denote the spatial average of a pore-scale quantity $A(\mathbf{x}, t)$ defined as in Eq. (2.56). Then, the spatial averaging of Eq. (2.72) leads to an upscaled equation:

$$\phi\frac{\partial \overline{c}}{\partial t} + \phi\nabla \cdot (\mathbf{V}\overline{c}) = \nabla \cdot (\mathbf{D}^*\nabla\overline{c}), \tag{2.74}$$

where $\mathbf{V}$ is the average macroscopic velocity and $\mathbf{D}^*$ is the dispersion coefficient.

2.4.5.2 *Derivation of coupling boundary conditions*
We are concerned with transport regimes in which the validity of the continuum-scale transport equation Eq. (2.74) breaks down in a subdomain $\Omega_p \subset \Omega^T_{pore}$ with boundary $\partial\Omega_p$ of the

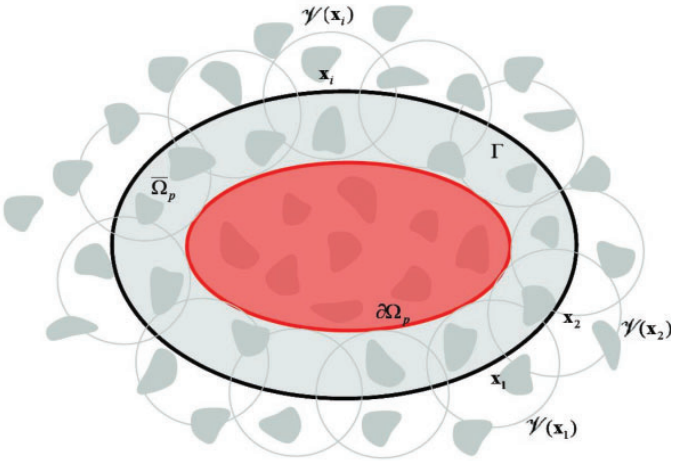

Figure 2.6 A schematic representation of the pore- and continuum-scale domains. The subdomain where continuum-scale representation breaks down is depicted in red. Its boundary is $\partial\Omega_p$. The boundary Γ is constructed as the locus of the centers of the family of averaging volumes $\mathscr{V}(\mathbf{x})$ whose envelope is $\partial\Omega_p$.

computational domain Ω. We define Γ to be the locus of the centers of the family of the averaging volumes $\mathscr{V}(\mathbf{x})$, whose envelope is $\partial\Omega_p$ as shown in Fig. 2.6. We denote $\overline{\Omega}_p$ the domain bounded by Γ. Let $A_{s\ell} = \overline{\Omega}_p \cap A_{s\ell}^T$.

Let $\overline{c}^{\leftarrow}$ denote the limiting value of $\overline{c}(\mathbf{x})$ as $\mathbf{x} \to \mathbf{x}^{\leftarrow} \in \Gamma$ from the *exterior* of $\overline{\Omega}_p$, and $\overline{c}^{\rightarrow} = \overline{c}(\mathbf{x}^{\rightarrow})$ as $\mathbf{x} \to \mathbf{x}^{\rightarrow} \in \Gamma$ from the *interior* of $\overline{\Omega}_p$. Since average concentration is a continuous function everywhere in Ω, it is continuous across Γ:

$$\overline{c}^{\leftarrow} = \overline{c}^{\rightarrow} \quad \text{for } |\mathbf{x}^{\rightarrow} - \mathbf{x}^{\leftarrow}| \to 0. \tag{2.75}$$

Let $\mathscr{V}^{in}(\mathbf{x}) := \mathscr{V}(\mathbf{x}) \cap \overline{\Omega}_p$ and $\mathscr{V}^{\text{out}}(\mathbf{x}) := \mathscr{V}(\mathbf{x}) \setminus \mathscr{V}^{\text{in}}(\mathbf{x})$ to form a partition of $\mathscr{V}$ where pore-scale is explicitly resolved and where only a continuum-scale representation exists, respectively (see Fig. 2.7). Then Eq. (2.75) can be written as:

$$\overline{c}^{\leftarrow} = \frac{1}{\phi|\mathscr{V}|}\int_{\mathscr{V}^{\text{in}}(\mathbf{x}^{\rightarrow})} c(\mathbf{y})\,\mathrm{d}\mathbf{y} + \frac{1}{\phi|\mathscr{V}|}\int_{\mathscr{V}^{\text{out}}(\mathbf{x}^{\rightarrow})} c(\mathbf{y})\,\mathrm{d}\mathbf{y}. \tag{2.76}$$

Expanding $c(\mathbf{y})$ into a Taylor series around the centroid $\mathbf{x}$, retaining the leading term, and substituting the result into Eq. (2.76) yields:

$$\overline{c}^{\leftarrow} = \frac{1}{\phi|\mathscr{V}|}\int_{\mathscr{V}^{\text{in}}(\mathbf{x}^{\rightarrow})} c(\mathbf{y})\,\mathrm{d}\mathbf{y} + \frac{|\mathscr{V}^{\text{out}}(\mathbf{x}^{\rightarrow})|}{\phi|\mathscr{V}|}c^{\rightarrow} \tag{2.77}$$

In a similar manner, one can show that a flux continuity condition across Γ can be written as:

$$\mathbf{n}\cdot(\mathbf{D}^*\nabla\overline{c}^{\leftarrow} - \phi\mathbf{v}\overline{c}^{\leftarrow}) = \frac{1}{|\mathscr{V}|}\mathbf{n}\cdot\int_{\mathscr{V}^{\text{in}}(\mathbf{x}^{\rightarrow})}(-\mathscr{D}\nabla c + \mathbf{v}c)\,\mathrm{d}\mathbf{y} + q_n, \tag{2.78}$$

where

$$q_n(\mathbf{x}) := \frac{1}{|\mathscr{V}|}\mathbf{n}\cdot\int_{\mathscr{V}^{\text{out}}(\mathbf{x})}(-\mathscr{D}\nabla c + \mathbf{v}c)\,\mathrm{d}\mathbf{y} \tag{2.79}$$

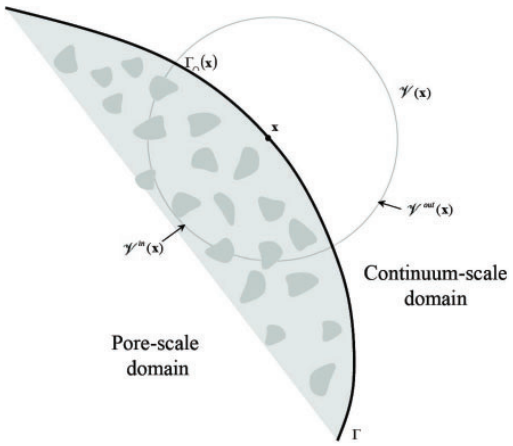

Figure 2.7 A schematic representation of the averaging procedure across the boundary separating pore- and continuum-scale representations. On the left of Γ pore-scale is fully resolved while on the right only a continuum-scale representation exists.

is an unknown flux through Γ. This flux serves as a coupling condition at the interface between pore- and continuum-scale subdomains.

The final form of the nonlinear coupled system of equations for the hybrid algorithm is:

$$\phi\frac{\partial\overline{c}}{\partial t}+\phi\nabla\cdot(\mathbf{V}\overline{c})=\nabla\cdot(\mathbf{D}^{*}\nabla\overline{c}),\quad \mathbf{x}\in\Omega\setminus\overline{\Omega}_{p}, \tag{2.80}$$

$$\frac{\partial c}{\partial t}+\nabla\cdot(\mathbf{v}c)=\mathscr{D}\nabla^{2}c,\quad \mathbf{x}\in\overline{\Omega}_{p}, \tag{2.81}$$

$$-\mathbf{n}\cdot\mathscr{D}\nabla c=0,\quad \mathbf{x}\in A_{s\ell}, \tag{2.82}$$

$$\mathbf{n}\cdot(-\mathscr{D}\nabla c+\mathbf{v}c)=q_{n},\quad \mathbf{x}\in\Gamma \tag{2.83}$$

$$\overline{c}^{\leftarrow}=\frac{1}{\phi|\mathscr{V}|}\int\limits_{\mathscr{V}^{\mathrm{in}}(\mathbf{x})}c\,\mathrm{d}\mathbf{y}+\frac{|\mathscr{V}^{\mathrm{out}}|}{\phi|\mathscr{V}|}c^{\rightarrow},\quad \mathbf{x}\in\Gamma, \tag{2.84}$$

$$\mathbf{n}\cdot(\mathbf{D}^{*}\nabla\overline{c}^{\leftarrow}-\phi\mathbf{V}\overline{c}^{\leftarrow})=q_{n}+\frac{1}{|\mathscr{V}|}\mathbf{n}\cdot\int\limits_{\mathscr{V}^{\mathrm{in}}(\mathbf{x}^{\rightarrow})}(-\mathscr{D}\nabla c+\mathbf{v}c)\,\mathrm{d}\mathbf{y},\quad \mathbf{x}\in\Gamma. \tag{2.85}$$

The interfacial conditions Eqs. (2.84) and (2.85) are reminiscent of the macroscopic Dirichlet and Neumann boundary conditions derived by the method of volume averaging in Prat (1989). While similar in spirit, our conditions do not require a closure approximation, relying on pore-scale simulations instead.

Coupling conditions for the Taylor dispersion problem are derived as a special case of our more general formulation in the following section.

2.4.5.3 *Taylor dispersion between parallel plates ($\mathscr{V}\cap\overline{\Omega}_{p}=\emptyset$)*

Whenever the average of a pore-scale variable $\xi(\mathbf{x})$ with $\mathbf{x}=(x_1,x_2,x_3)\in\Omega_1\times\Omega_2\times\Omega_3$ is defined by integrating one of the independent variables x_i over Ω_i, $i=1,2,3$, the dimensionality of the

correspondent continuum-scale equation is reduced. An example is the problem of Taylor dispersion between two infinite parallel plates separated by the distance $2H$. Now $\Omega_1 = (-\infty, +\infty)$, $\Omega_2 = (-H, H)$, and the average of a generic pore-scale variable is defined as:

$$\xi(x) = \frac{1}{2H} \int_{-H}^{H} \xi(x, y)\, \mathrm{d}y. \tag{2.86}$$

This allows one to derive a one-dimensional effective equation starting from a two-dimensional pore-scale problem. In such situation, $\mathscr{V} = \mathscr{V}^{\text{out}}$ and $\mathscr{V}^{\text{in}} = \emptyset$. The boundary Γ reduces to a point and to a vertical segment of length $2H$ on the continuum- and pore-scale subdomains, respectively. Since $\phi = 1$, the general coupling conditions for state variables and fluxes at the boundary Γ established by Eqs. (2.84) and (2.85) simplify to:

$$\overline{c}^{\leftarrow} = c^{\rightarrow}, \qquad \mathbf{x} \in \Gamma, \tag{2.87}$$

$$\mathbf{n} \cdot (\mathbf{D}^* \nabla \overline{c}^{\leftarrow} - \phi \mathbf{V} \overline{c}^{\leftarrow}) = q_n, \qquad \mathbf{x} \in \Gamma. \tag{2.88}$$

These conditions establish that pore-scale concentration and flux are constant along the boundary and equal to the continuum-scale value on the boundary exterior.

2.4.5.4 *Hybrid algorithm*

Solving the nonlinear coupled system Eqs. (2.80)–(2.85) reduces to finding zeros of a system of equations in the form:

$$F(q_n, c^{\rightarrow}) = 0, \quad G(q_n, c^{\rightarrow}) = 0, \tag{2.89}$$

where

$$F(q_n, c^{\rightarrow}) = \mathbf{n} \cdot (\mathbf{D}^* \nabla \overline{c}^{\leftarrow} - \phi \mathbf{V} \overline{c}^{\leftarrow}) - \frac{1}{|\mathscr{V}|} \int\limits_{\mathscr{V}^{\text{in}}(\mathbf{x}^{\rightarrow})} \mathbf{n} \cdot (-\mathscr{D} \nabla c + \mathbf{v} c)\, \mathrm{d}\mathbf{y} - \frac{|\Gamma(\mathbf{x}^{\rightarrow})|}{|\mathscr{V}|} q_n, \tag{2.90}$$

$$G(q_n, c^{\rightarrow}) = \overline{c}^{\leftarrow} - \frac{1}{\phi |\mathscr{V}|} \int\limits_{\mathscr{V}^{\text{in}}(\mathbf{x})} c\, \mathrm{d}\mathbf{y} - \frac{|\mathscr{V}^{\text{out}}|}{\phi |\mathscr{V}|} c^{\rightarrow}. \tag{2.91}$$

The hybrid pore-scale/continuum-scale algorithm can be formulated as follows

- Initialization. At timestep T^N, $c(t = T^N)$ and $\overline{c}(t = T^N)$ are known.
- Guess for flux. Make a guess for q_n. This imposes the Robin condition Eq. (2.83) at interface Γ.
- Pore-scale evolution. The pore-scale equation Eq. (2.81), supplemented with boundary condition Eq. (2.82), is evolved from T^N to T^{N+1}.
- Evaluation of boundary integrals. The right hand side of Eq. (2.91) is evaluated together with the integral term in Eq. (2.85). The latter imposes the Robin condition Eq. (2.85) at the interface Γ.
- Continuum-scale evolution. The continuum-scale concentration $\overline{c}$ is evolved from T^N to T^{N+1} by Eq. (2.80).
- Continuum-scale concentration evaluation. The function G is computed by means of Eq. (2.91).
- Convergence check and iteration. For a given tolerance ϵ, if $|G(q_n, c_\Gamma)| > \epsilon$, the Broyden method (or another root-finding algorithm) is used to refine the guess of q_n and go to step 2. If $|G(q_n, c_\Gamma)| \leq \epsilon$, then the convergence is reached. March forward in time ($N := N + 1$) and go to step 1.

2.5 CONCLUSIONS

Our study leads to the following major conclusions:

- While capable of describing many processes at a variety of different scales, macroscopic models might breakdown. We established conditions under which macroscopic reaction-diffusion

equations (RDEs) provide an adequate averaged description of pore-scale processes. We showed that the range of applicability of macroscopic RDEs and various transport regimes can be described by a phase diagram in a space spanned by the dimensionless Damköhler number and a scale separation parameter. This was accomplished by upscaling a system of nonlinear diffusion-reaction equations at the pore-scale by means of volume averaging technique. For physical phenomena that do not satisfy such conditions, an upscaled (local) equation does not generally exist and integro-differential (non-local in space and time) alternatives or hybrid models must be used instead.

- The previous result was generalized by considering macroscopic advection-dispersion-reaction equations (ADREs). The method of multiple-scale expansion was used to upscale to the continuum (Darcy) scale a pore-scale advection-diffusion equation with nonlinear reactions entering through a boundary condition on the fluid-solid interfaces. The range of applicability of macroscopic ADREs can be described with a phase diagram in the (Da, Pe)-space (where Da and Pe are Damköhler and Péclet numbers, respectively). The latter is parametrized with a scale-separation parameter, defined as the ratio of characteristic lengths associated with the pore-and macro-scales. This phase diagram revealed that transport phenomena dominated at the pore-scale by reaction processes do not lend themselves to macroscopic descriptions and effective parameters do not generally exist. These results generalize our previous findings relative to RDEs and suggest that they are universal, i.e., independent of the choice of an upscaling technique.
- When the validity of continuum-scale models cannot be ascertained a priori in small portions of the computational domain, hybrid models that couple pore- and continuum-scale representations can be used. We developed a general intrusive hybrid algorithm to incorporate pore-scale effects into continuum models of reactive transport in fractured media. This formulation is based on overlapping the pore- and continuum-scale representations and therefore requires the modification of some coefficients in the discretized system of equations. We applied our algorithm to model Taylor dispersion in a planar fracture with chemically reactive walls. Existing analytical solutions served as validation. The hybrid model formulation reduces to a zero-finding algorithm for a vector function: this suggests its high applicability to a wide variety of problems and numerical schemes. The proposed method is capable of handling highly localized heterogeneities, which provides a considerable improvement in accuracy and enables one to properly capture the pore-scale physics.
- A desirable feature of a hybrid model is its ability to be easily incorporated into existing (legacy) codes/software. Even though not necessary to this purpose, a formalization that is not intrusive would render such a task much easier. Therefore we developed an alternate formalization for the hybridization that is nonintrusive and a priori does not require mesh refinement on the continuum-scale subdomain to match the mesh dimension on the pore-scale subdomain.

ACKNOWLEDGEMENT

This research was supported by the Office of Science of the U.S. Department of Energy (DOE) under the Scientific Discovery through Advanced Computing (SciDAC).

REFERENCES

Acharya, R.C., der Zee, S.E.A.T.M.V. & Leijnse, A. (2005) Transport modeling of nonlinearly adsorbing solutes in physically heterogeneous pore networks. *Water Resources Research*, 41, W02020.

Adler, P.M. (1992) *Porous Media: Geometry and Transports*. Butterworth-Heinemann, New York.

Auriault, J.L. (2009) On the domain of validity of Brinkman's equation. *Transport Porous Media*, 79, 215–223.

Auriault, J.L. & Adler, P.M. (1995) Taylor dispersion in porous media: Analysis by multiple scale expansions. *Advances in Water Resources*, 18 (4), 217–226.

Auriault, J.L., Geindreau, C. & Boutin, C. (2005) Filtration law in porous media with poor separation of scales. *Transport Porous Media*, 60, 89–108.

Battiato, I. & Tartakovsky, D.M. (2010) Applicability regimes for macroscopic models of reactive transport in porous media. *Journal of Contaminant Hydrology*, Available from: doi:10.1016/j.jconhyd.2010.05.005.

Battiato, I., Tartakovsky, D.M., Tartakovsky, A.M. & Scheibe, T.D. (2009) On breakdown of macroscopic models of mixing-controlled heterogeneous reactions in porous media. *Advances in Water Resources*, 32: 1664–1673.

Battiato, I., Tartakovsky, D.M., Tartakovsky, A.M. & Scheibe, T.D. (2011) Hybrid models of reactive transport in porous and fractured media. *Advances in Water Resources*, Available from: doi:10.1016/j.advwatres.2011.01.012.

Brenner, H. (1987) *Transport Processes in Porous Media*, New York, McGraw-Hill.

Brinkman, H.C. (1949) A calculation of the viscous force exerted by a flowing fluid on a dense swarm of particles. *Applied Science Research*, A1, 27–34.

Broyda, S., Dentz, M. & Tartakovsky, D.M. (2010) Probability density functions for advective-reactive transport in radial flow. *Stochastic Environmental Research and Risk Assessment*, Available from: doi:10.1007/s00477–010–0401–4.

Christie, M. (1996) Upscaling for reservoir simulation. *Journal of Petroleum Technology*, 48, 1004–1010.

Darcy, H. (1856) Les fontaines publiques de la Ville de Dijon, Paris, *Victor Darmon*.

de Marsily, G. (1986) *Quantitative Hydrogeology*. San Diego, California, Academic Press.

Duijn, C.J.V. & Pop, I.S. (2004) Crystal dissolution and precipitation in porous media: Pore-scale analysis. *Journal für die Reine und Angewandte Mathematik*, 577, 171–211.

Durlofsky, L.J. & Brady, J.F. (2009) Analysis of the Brinkman equation as a model for flow in porous media. *Physics of Fluids*, 30 (11), 3329–3341.

Efendief, Y. & Durlofsky, L.J. (2003) A generalized convection-diffusion model for subgrid transport in porous media. *Multiscale Modeling and Simulation*, 1 (3), 504–526.

Goyeau, B., Benihaddadene, T., Gobin, D., & Quintard, M. (1997) Averaged momentum equation for flow through a nonhomogeneous porous structure. *Transport Porous Media*, 28, 19–50.

Gray, W.G. & Miller, C.T. (2005) Thermodynamically constrained averaging theory approach for modeling flow and transport phenomena in porous medium systems: 1. Motivation and overview. *Advances in Water Resources*, 28 (2), 161–180.

Hesse, F., Radu, F.A., Thullner, M. & Attinger, S. (2009) Upscaling of the advection–diffusion–reaction equation with Monod reaction. *Advances in Water Resources*, 32, 1336–1351.

Hornung, U. (1997) *Homogenization and Porous Media*, New York, Springer.

Kechagia, P.E., Tsimpanogiannis, I.N., Yortsos, Y.C. & Lichtner, P.C. (2002) On the upscaling of reaction-transport processes in porous media with fast or finite kinetics. *Chemical Engineering Science*, 57 (13), 2565–2577.

Knabner, P., Duijn, C.J.V. & Hengst, S. (1995) An analysis of crystal dissolution fronts in flows through porous media. Part 1: Compatible boundary conditions. *Advances in Water Resources*, 18 (3), 171–185.

Knutson, C., Valocchi, A. & Werth, C. (2007) Comparison of continuum and pore-scale models of nutrient biodegradation under transverse mixing conditions. *Advances in Water Resources*, 30 (6–7), 1421–1431.

Kundu, P.K. & Cohen, I.M. (2008) *Fluid Mechanics*, 4th edition. San Diego, Elsevier.

Langlo, P. & Espedal, M.S. (1994) Macrodispersion for two-phase, immiscible flow in porous media. *Advances in Water Resources*, 17, 297–316.

Leemput, P., Vandekerckhove, C., Vanroose, W. & Roose, D. (2007) Accuracy of hybrid lattice Boltzmann/finite difference schemes for reaction diffusion systems. *Multiscale Modeling and Simulation* 6 (3), 838–857.

Lévy, T. (1983) Fluid flow through an array of fixed particles. *International Journal of Engineering Science*, 21, 11–23.

Li, L., Peters, C. & Celia, M. (2006) Upscaling geochemmical reaction rates sing pore-scale network modeling. *Advances in Water Resources*, 29, 1351–1370.

Lichtner, P.C. & Tartakovsky, D.M. (2003) Upscaled effective rate constant for heterogeneous reactions. *Stochastic Environmental Research and Risk Assessment*, 17 (6), 419–429.

Maloy, K.J., Feder, J., Boger, F. & Jossang, T. (1998) Fractal structure of hydrodynamic dispersion in porous media. *Physical Review Letter*, 61 (82), 2925.

Marušić-Paloka, E. & Piatnitski, A. (2005) Homogenization of a nonlinear convection-diffusion equation with rapidly oscillating coefficients and strong convection. *Journal of the London Mathematical Society*, 2 (72), 391–409.

Mikelić, A., Devigne, V. & Van Duijn, C.J. (2006) Rigorous upscaling of the reactive flow through a pore, under dominant Peclet and Damköhler numbers. *SIAM Journal on Mathematical Analysis*, 38 (4), 1262–1287.

Morse, J.W. & Arvidson, R.S. (2002) The dissolution kinetics of major sedimentary carbonate minerals. *Earth Science Reviews*, 58, 51–84.

Neuman, S.P. (1977) Theoretical derivation of Darcy's law. *Acta Mecanica*, 25, 153–170.

Neuman, S.P. & Tartakovsky, D.M. (2009) Perspective on theories of anomalous transport in heterogeneous media. *Advances in Water Resources*, 32 (5), 670–680.

Nitsche, L.C. & Brenner, H. (1989) Eulerian kinematics of flow through spatially periodic models of porous media. *Archive for Rational Mechanics and Analysis*, 107(3), 225–292.

Ochoa-Tapia, J.A., Stroeve, P. & Whitaker, S. (1991) Facilitated transport in porous media. *Chemical Engineering Science*, 46, 477–496.

Peter, M.A. (2007) Homogenization in domains with evolving microstructure. *Comptes Rendus Mécanique* 335: 357–362.

Prat, M. (1989) On the boundary conditions at the macroscopic level. *Transport Porous Media*, 4, 259–280.

Sanchez-Palencia, E. & Zaoui, A. (1989) Homogenization techniques for composite media. In: Sanchez-Palencia, E. & Zaoui, A. (eds.). *Lectures Delivered at the CISM International Center for Mechanical Sciences, July 1–5 1985, Udine, Italy*. Berlin, Heidelberg, Springer. *Lecture Notes in Physics*, 272, 1987.

Shapiro, M. & Brenner, H. (1986) Taylor dispersion of chemically reactive species: Irreversible first-order reactions in bulk and on boundaries. *Chemical Engineering Science*, 41 (6), 1417–1433.

Shapiro, M. & Brenner, M. (1988) Dispersion of a chemically reactive solute in a spatially periodic model of a porous medium. *Chemical Engineering Science*, 43 (3), 551–571.

Shapiro, M., Fedou, R., Thovert, J. & Adler, P.M. (1996) Coupled transport and dispersion of multicomponent reactive solutes in rectilinear flows. *Chemical Engineering Science*, 51 (22), 5017–5041.

Steefel, C.I., DePaolo, D.J. & Lichtner, P.C. (2005) Reactive transport modeling: An essential tool and a new research approach for the Earth sciences. *Earth Planetary Science Letters*, 240, 539–558.

Tartakovsky, A.M., Meakin, P., Scheibe, T.D. & West, R.M.E. (2007) Simulation of reactive transport and precipitation with smoothed particle hydrodynamics. *Journal of Computational Physics*, 222, 654–672.

Tartakovsky, A.M., Redden, G., Lichtner, P.C., Scheibe, T. D. & Meakin, P. (2008) Mixing-induced precipitation: Experimental study and multi-scale numerical analysis. *Water Resources Research*, 44, W06S04, doi:10.1029/2006WR005725.

Tartakovsky, A.M., Tartakovsky, D.M. & Meakin, P. (2008) Stochastic Langevin model for flow and transport in porous media. *Physical Review Letters*, 101(4), 044502. Available from: doi:10.1103/PhysRevLett.101.044502.

Tartakovsky, A.M., Tartakovsky, D.M., Scheibe, T.D. & Meakin, P. (2007) Hybrid simulations of reaction-diffusion systems in porous media. *SIAM Journal of Scientific Computing*, 30 (6), 2799–2816.

Tartakovsky, D.M., Dentz, M. & Lichtner, P.C. (2009) Probability density functions for advective-reactive transport in porous media with uncertain reaction rates. *Water Resources Research*, 45, W07414. Available from: doi:10.1029/2008WR007383.

van Noorden, T.L. & Pop, I.S. (2008) A Stefan problem modelling crystal dissolution and precipitation. *IMA Journal of Applied Mathematics* 73 (2), 393–411.

Walther, J.H., Werder, T., Jaffe, R.L. & Koumoutsakos, P. (2004) Hydrodynamic properties of carbon nanotubes. *Physical Review E*, 69, 062201.

Whitaker, S. (1999) *The Method of Volume Averaging*. Netherlands, Kluwer Academic Publishers.

Wood, B.D. & Ford, R.M. (2007) Biological processes in porous media: From the pore scale to the field. *Advances in Water Resources*, 30 (6–7), 1387–1391.

Wood, B.D., Radakovich, K. & Golfier, F. (2007) Effective reaction at a fluid-solid interface: Applications to biotransformation in porous media. *Advances in Water Resources*, 30 (6–7), 1630–1647.